

Geochemistry, Geochronology and Isotopic Evolution of the Chewore–Rufunsa Terrane, Southern Irumide Belt: a Mesoproterozoic Continental Margin Arc

SIMON P. JOHNSON^{1*}, BERT DE WAELE^{2†}, FRANCIS TEMBO³, CRISPIN KATONGO^{3‡}, KENICHIRO TANI¹, QING CHANG¹, TSUYOSHI IIZUKA^{4§} AND DANIEL DUNKLEY⁵

¹INSTITUTE FOR RESEARCH ON EARTH EVOLUTION, JAPAN AGENCY FOR MARINE–EARTH SCIENCE AND TECHNOLOGY, 2-15 NATSUSHIMA-CHO, YOKOSUKA, KANAGAWA-KEN, 237-0061, JAPAN

²TECTONICS SPECIAL RESEARCH CENTRE, SCHOOL OF EARTH AND GEOGRAPHICAL SCIENCES, UNIVERSITY OF WESTERN AUSTRALIA, 35 STIRLING HIGHWAY, CRAWLEY, WA 6009, AUSTRALIA

³SCHOOL OF MINES, GEOLOGY DEPARTMENT, UNIVERSITY OF ZAMBIA, PO BOX 32379, LUSAKA, ZAMBIA

⁴LABORATORY FOR PLANETARY SCIENCES, TOKYO INSTITUTE OF TECHNOLOGY, 2-1-12 O-OKAYAMA, MEGURO, TOKYO, 152-8551, JAPAN

⁵NATIONAL INSTITUTE OF POLAR RESEARCH, 9-10 KAGA 1-CHOME, ITABASHI-KU, TOKYO 173-8515, JAPAN

RECEIVED AUGUST 28, 2006; ACCEPTED APRIL 5, 2007

The southern Irumide Belt (SIB) is an ENE–WSW-trending, late Mesoproterozoic orogenic belt located between the Congo–Tanzania–Bangweulu (CTB) and Kalahari cratons in central southern Africa. It is separated from the late Mesoproterozoic Irumide Belt (IB) to the north by Permo–Triassic graben, raising the possibility that the younger rifts reactivated a suture between the two belts that has been rendered cryptic as a result of younger Karoo cover. Both belts are dominated by calc-alkaline gneisses, but in addition the SIB contains abundant metavolcanic and metasedimentary rocks. In this study we present detailed geochemical, isotopic and geochronological data for volcanic and plutonic lithologies from the southernmost part of the SIB, the Chewore–Rufunsa Terrane. This terrane comprises a wide variety of supracrustal to mid-crustal rocks that have major- and trace-element compositions similar to magmas formed in present-day subduction zones. Chondrite-normalized rare earth element (REE) profiles and whole-rock Sm–Nd isotope compositions indicate that the parental supra-subduction melts interacted

with, and were contaminated by sialic continental crust, implying a continental-margin-arc setting. Secondary ionization mass spectrometry dating of magmatic zircon has yielded crystallization ages between c. 1095 and 1040 Ma, similar to elsewhere in the SIB. U–Pb dating and in situ Lu–Hf isotopic analyses of abundant xenocrystic zircon extracted from the late Mesoproterozoic granitoids indicate that the contaminant continental basement was principally Palaeoproterozoic in age and had a juvenile isotopic signature at the time of its formation. These data are in contrast to those for the IB, which is characterized by younger, c. 1020 Ma, calc-alkaline gneisses that formed by the direct recycling of Archaean crust without significant addition of any juvenile material. We suggest that the SIB developed by the subduction of oceanic crust under the margin of an unnamed continental mass until ocean closure at c. 1040 Ma. Subsequent collision between the SIB and the CTB margin led to the cessation of magmatism in the SIB and the initiation of compression and crustal melting in the IB.

*Corresponding author. Present address: Geological Survey of Western Australia, Mineral House, 100 Plain Street, East Perth, WA 6004, Australia. Tel: +61 8 9222 3127. Fax: +61 8 9222 3633.

E-mail: simon.johnson2@doir.wa.gov.au

†Present address: British Geological Survey, Keyworth, Nottingham NG12 5GG, UK.

‡Deceased.

§Present address: Earthquake Research Institute, University of Tokyo, Yayoi 1-1-1, Bunkyo-Ku, Tokyo 113-0032, Japan.

© The Author 2007. Published by Oxford University Press. All rights reserved. For Permissions, please e-mail: journals.permissions@oxfordjournals.org

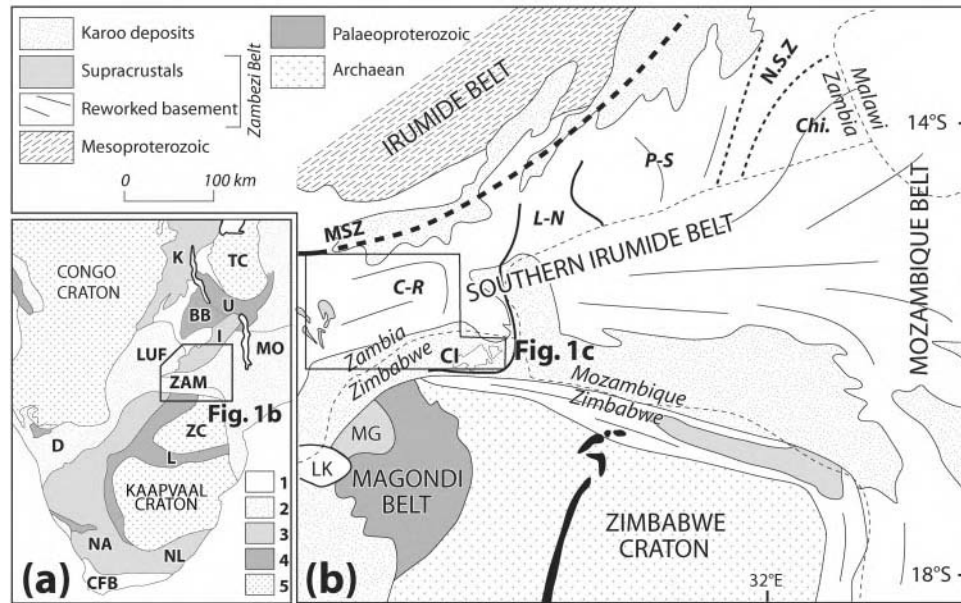


Fig. 1. (a) Simplified tectonic map of Africa after Hanson (2003). 1, Phanerozoic Belts; 2, Neoproterozoic–Cambrian Belts; 3, Mesoproterozoic Belts; 4, Palaeoproterozoic Belts; 5, Archaean Cratons. BB, Bangweulu Block; CFB, Cape Fold Belt; D, Damara Belt; I, Irumide Belt; K, Kibaran Belt; LUF, Lufilian Belt; L, Limpopo Belt; MO, Mozambique Belt; NA, Namaqua Belt; NL, Natal Belt; TC, Tanzania Craton; U, Ubendian Belt–Usagaran Belt; ZAM, Zambezi Belt; ZC, Zimbabwe Craton. (b) Simplified geological map [area shown by box in (a)] of central southern Africa after Johnson *et al.* (2005), showing the main lithotectonic terrane subdivisions of the Southern Irumide Belt (after Johnson *et al.* 2006). Area of main map (c) is outlined. Chi, Chipata Terrane; CI, Chewore Inliers; C-R, Chewore–Rufunsa Terrane; LK, Lake Kariba; L-N, Luangwa–Nyimba Terrane; MG, Makuti Group; MSZ, Mwembeshi Shear Zone; NSZ, Nyamadzi Shear Zone; P-S, Petauke–Sinda Terrane. (c) Geological map of the Chewore–Rufunsa Terrane [box in (b)] showing the distribution of the four (a, Chakwenga; b, Chongwe; c, Chewore; d, Ikondo) supracrustal meta-mafic to meta-felsic volcano-plutonic complexes. Solid geology of the Zambian side of the complex is taken from the 1:250 000 Geological Survey of Zambia map series, Sheet No. SD-35-16 (Barr, 1998). The geology of the Zimbabwean side of the complex is compiled from Goscombe *et al.* (1994, 1998, 2000) and Johnson & Oliver (2000, 2004). Most of the mega-scale structures shown on the map (folds and ductile faults) are Pan-African in age (late Neoproterozoic to Cambrian) and have overprinted and obliterated any structures associated with the original Mesoproterozoic tectonomagmatic environment. Local UTM grid coordinates are prefixed by 35L and are in the ARC1950 datum. Locations of Figs 2–4 are outlined by boxes. LZNP, Lower Zambezi National Park.

KEY WORDS: *geochemistry; Mesoproterozoic; SHRIMP zircon U–Pb dating; Sm–Nd isotopes; Southern Irumide Belt*

INTRODUCTION

Central southern Africa is a complex region of Archaean cratons and enveloping orogenic belts that range in age from Palaeoproterozoic to Cambrian (Fig. 1a). Until recently, it was presumed that these cratons were mostly assembled in the mid- to late Mesoproterozoic during a sub-Saharan-wide ‘Kibaran Orogeny’ (Hanson, 2003). However, analysis of the geochronological and sparse geochemical data from these various Mesoproterozoic belts has demonstrated that magmatism and compressional tectonics occurred at distinctly different times in different belts, and that most of the belts presumably owe their character to distinct and unrelated geological processes (De Waele *et al.*, 2003; Johnson *et al.*, 2005). The majority of the central African Mesoproterozoic belts are dominated by felsic calc-alkaline gneisses, but it has yet to be determined whether the protoliths of these gneisses formed by juvenile or crustal recycling processes. For

instance, the calc-alkaline rocks may have formed in a continental-margin arc, or by accretion of juvenile or mature oceanic arcs to the continent margin, or by the complete tectonic recycling of older calc-alkaline basement gneisses in a hot, wide, Himalayan-style collisional orogen. In this study we present a detailed integrated geochemical, isotopic and geochronological investigation of part of one Mesoproterozoic Belt, the Southern Irumide Belt, which is situated between the Greater Congo Craton (the combined Congo–Tanzania–Bangweulu Craton or CTB) and the Kalahari Craton (Fig. 1a). We provide evidence to indicate that this belt formed as part of a continental-margin arc on the margin of an unnamed continent that subsequently collided with the CTB craton during the late Mesoproterozoic.

REGIONAL GEOLOGY

The Southern Irumide Belt (SIB) (Fig. 1b) is a lithologically varied and locally multiply deformed belt of metasedimentary, metavolcanic and metaplutonic rocks that are distinct from the monotonous granitoid gneisses that form

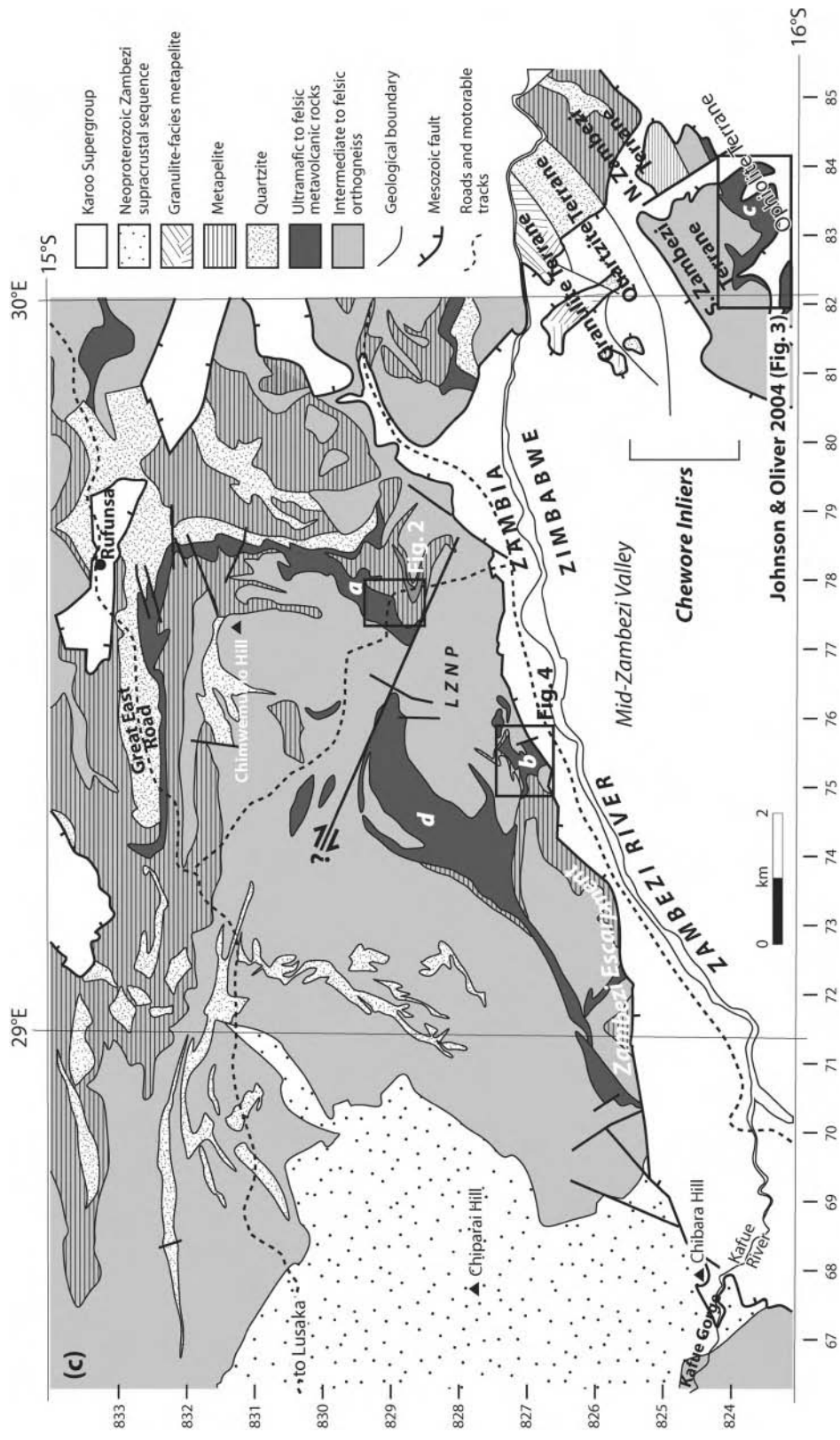


Fig. 1. Continued.

much of the adjacent Irumide Belt (*sensu stricto*) (De Waele, 2005; Johnson *et al.*, 2005, 2006; De Waele *et al.*, 2006b). The SIB is exposed in southern Zambia, northern Zimbabwe, northern Malawi and western Mozambique (Fig. 1a–c) but the contact with the Irumide Belt is obscured by a Permo-Triassic ‘Karoo’ graben, raising the possibility that these younger rifts reactivate and mask a cryptic suture between the two (Johnson *et al.*, 2006). Based on lithostratigraphy, structure and metamorphic characteristics, Mapani *et al.* (2001, 2004) provisionally subdivided the SIB in Zambia into several lithologically distinct terranes bounded by ductile shear zones. This architecture was used as the basis for an extensive U–Pb sensitive high-resolution ion microprobe (SHRIMP) zircon geochronological study of the region (Johnson *et al.*, 2006) that resulted in some modifications, as shown in Fig. 1b. The Chewore–Rufunsa Terrane (Fig. 1b), the focus of the present study, comprises late Mesoproterozoic calc-alkaline gneisses and metavolcanic rocks. Major- and trace-element and rare earth element (REE) geochemical analyses from the Chewore Inliers of northern Zimbabwe indicate that the lithologies formed via supra-subduction-zone magmatic processes (Oliver *et al.*, 1998; Johnson & Oliver, 2000, 2004); however, there are no published isotopic data to support this interpretation. The structurally overlying Luangwa–Nyimba Terrane (Fig. 1b) to the east is dominated by calcareous, psammitic and pelitic metasedimentary rocks, and the Petauke–Sinda Terrane to the east of that (Fig. 1b) consists of a suite of late Mesoproterozoic calc-alkaline plutonic rocks and late Cambrian post-tectonic granites and syenites (Johnson *et al.*, 2006). The easternmost terrane in Zambia, the Chipata Terrane, is composed of variably deformed high-temperature mafic and felsic granulite including meta-igneous lithologies (charnockite and charno-enderbite) and various sillimanite-bearing metasedimentary lithologies of Palaeoproterozoic and Mesoproterozoic age (Johnson *et al.*, 2006). In the poorly studied regions of northern Malawi and western Mozambique, the nature of the SIB is obscure and the locations of the terrane boundaries are unknown; however, various Rb–Sr and Sm–Nd whole-rock–mineral isochrons, zircon Pb–evaporation ages and unpublished U–Pb SHRIMP zircon ages indicate the presence of similar Mesoproterozoic protoliths (Kröner *et al.*, 1997; Evans *et al.*, 1999; Mäkitie *et al.*, 2006; Mänttari *et al.*, 2006). Metamorphism throughout the SIB in Zambia is generally high-temperature (>850°C) and low-pressure (<4.5 kbar) in nature and has been dated between 1.07 and 1.04 Ga (Goscombe *et al.*, 1998, 2000; Schenk & Appel, 2001, 2002; Cox *et al.*, 2002; Johnson & Oliver, 2004; Johnson *et al.*, 2006); however, parts of the SIB were reworked under high- to very high-pressure conditions (~20 kbar) during the Neoproterozoic–Cambrian Pan-African Zambezi Orogeny (*c.* 550–515 Ma) (John *et al.*, 2004; Johnson *et al.*, 2004;

Johnson *et al.*, 2005). This multiple reworking has completely obliterated any pre Pan-African structures and metamorphic assemblages, making the interpretation of Mesoproterozoic events especially cryptic.

In contrast, the Irumide Belt (*sensu stricto*; IB) comprises a basement of granitoid gneiss emplaced between 2.05 and 1.93 Ga overlain by a supracrustal sequence, the Muva Supergroup, at *c.* 1.87–1.86 Ga (De Waele & Fitzsimons, 2004). Both basement gneiss and Muva Supergroup were locally intruded by small granitoid bodies at 1.65–1.55 Ga and later by voluminous K-feldspar megacrystic granitoid batholiths between 1.05 and 0.95 Ga (De Waele, 2005; De Waele *et al.*, 2006b). These late Mesoproterozoic calc-alkaline granitoids were derived by recycling of basement gneisses without addition of any juvenile material (De Waele *et al.*, 2006a). Medium-pressure, high-temperature metamorphism (~8 kbar at 850°C) and contractional deformation accompanied the main magmatic event at *c.* 1.02 Ga (Daly, 1986; De Waele, 2005) producing strong NE–SW structural trends.

GEOLOGY OF THE CHEWORE–RUFUNSA TERRANE

The Chewore–Rufunsa (C–R) Terrane is exposed along the deeply incised Zambian Zambezi Valley fault escarpment and within isolated and remote basement horsts (known as the Chewore Inliers) that sit within the Mid Zambezi Valley of northern Zimbabwe (Fig. 1c). Mapping by the Zambian and Zimbabwean (formally Rhodesian) Geological Surveys (Goscombe *et al.*, 1994, 1998, 2000; Barr, 1998) has revealed the presence of a wide variety of mafic to felsic gneisses, K-feldspar augen gneisses, metapelites and abundant quartzites (Fig. 1c). The metamorphic grade increases dramatically from greenschist facies in the northern part of the terrane around Rufunsa (Barr, 1998) to high- to moderate-pressure amphibolite facies and local granulite facies in the south (Goscombe *et al.*, 1998, 2000; Johnson & Oliver, 2000, 2004). A striking feature of the terrane is the presence of four mafic to felsic complexes, composed of plutonic and volcano-sedimentary rocks, here named the Chakwenga, Chongwe, Chewore (the Ophiolite Terrane of Oliver *et al.* 1998) and Ikondo complexes (Fig. 1c).

The Chewore Complex

Detailed investigations of the Chewore Inliers (Goscombe *et al.*, 1998, 2000; Oliver *et al.*, 1998; Johnson & Oliver, 2000, 2004) have provided a wealth of geochemical and geochronological data. The Chewore Inliers have been divided into four fault-bounded lithotectonic slices [termed terranes by Goscombe *et al.* (1994) and Oliver *et al.* (1998)], the Granulite, Quartzite, Zambezi and Ophiolite (Chewore Complex of this study) terranes. The Chewore Complex, one of the four regional mafic to felsic complexes in the

C–R Terrane, comprises a variable suite of rocks ranging from ultramafic to felsic in composition, which exhibit the geochemical signatures of a marginal basin ophiolite [the Chewore Ophiolite of Oliver *et al.* (1998) and Johnson & Oliver (2000)] and a low-K tholeiitic island arc [the Kaourera Arc of Johnson & Oliver (2004)]. Low-strain zones in both the ophiolite and arc suites reveal primary volcanic features such as vesicular textures and pillows, indicating that parts of this complex are of supracrustal origin (Johnson & Oliver, 2000, 2004). SHRIMP dating of igneous zircon from a plagiogranite dyke within the Chewore Ophiolite and a metadacite in the Kaourera Arc indicate ocean crust formation at *c.* 1393 Ma (Oliver *et al.*, 1998) and island arc formation at *c.* 1082 Ma (Johnson & Oliver, 2004), respectively. Felsic to intermediate orthogneisses that make up the Zambezi Terrane and intrude metasediments of the Granulite Terrane also display arc-like geochemical affinities (Johnson & Oliver, 2004) and crystallization ages similar to the arc rocks at 1071 Ma and 1083 Ma (Goscombe *et al.*, 2000), leading to the interpretation that the different Chewore Inlier terranes represent different levels within a single arc complex (Johnson & Oliver, 2004).

The Chakwenga Complex

Lithologies of the Chakwenga Complex are best exposed along the Chakwenga River and its tributaries within the Lower Zambezi National Park (Figs 1c and 2). All lithologies have been metamorphosed to at least lower- to mid-amphibolite facies during the Neoproterozoic to Cambrian Zambezi orogeny and carry a strong south-dipping planar and SE-plunging linear fabric (Fig. 2), defined by the alignment of biotite and hornblende and/or quartz–feldspar aggregates. The complex can be divided into two main units, fine-grained mafic to intermediate mylonitic gneiss and medium- to coarse-grained hornblende gneiss and metagabbro. The northern part of the complex (north of UTM 8290; Fig. 2) is dominated by fine-grained amphibolitic mylonitic gneiss composed of quartz, plagioclase (\pm K-feldspar), biotite and hornblende (Figs 2 and 3a) with minor hornblende gneiss in the extreme NE of the mapping area (Fig. 2). Sparse felsic rocks contain fine-grained quartz and feldspar with minor biotite and in low-strain zones are commonly observed to contain relict tuffaceous textures (e.g. GR 0780867–8292595–sample 38). Garnet-bearing muscovite schist and quartzite layers containing intense internal isoclinal to tight shear folds are common.

To the south of UTM 8290 (Fig. 2), medium- to coarse-grained hornblende gneiss and metagabbro dominate (Figs 2 and 3b). The hornblende gneisses are composed of flattened and aligned feldspar, hornblende and biotite with little to no free quartz, and the metagabbros are composed of elongate, aligned hornblende and feldspar. In low-strain zones some of the metagabbros display

relict sub-cumulate textures. At GR 0779614–8288973, a mylonitized fine- to medium-grained hornblende gneiss (sample 45a) contains thin (usually less than 10 cm wide) boudinaged lenses and layers (0.5–5 m in length) of coarse-grained, mildly strained metagabbro (sample 45b; Fig. 3b). These lenses and layers make up \sim 30% of the outcrop and have sharp, finer-grained (but not strained) margins with the surrounding gneiss, suggesting that they may represent relict dykes. The presence of thrust faults is interpreted on the basis of decimetre-wide ductile shear zones that are associated with distinct changes in lithology.

The Chongwe Complex

The Chongwe Complex is best exposed along the Chongwe and Chowe (also locally known as Chiawa) rivers that deeply dissect the Zambezi fault escarpment in Zambia (Figs 1 and 4). Lithologies in both river sections have attained, at least, upper amphibolite-facies conditions during the late Neoproterozoic to Cambrian (John *et al.*, 2004) and garnet is an abundant phase in rocks of variable compositions.

The Chongwe River section (Figs 4 and 5a) is dominated by garnet-bearing and occasionally biotite-rich amphibolites that are interbanded with metre- to decimetre-thick leucocratic, garnet–feldspar–quartz–biotite gneiss (Fig. 3c). Amphibolite predominates over the felsic gneiss throughout the section but in localized zones up to 100 m in width, the felsic gneiss can form up to 75% of the rock volume. All lithologies carry a strong planar tectonic fabric and the contacts between the units are sharp with no apparent gradational boundaries.

The Chowe River section (Fig. 5b) exposes similar mylonitic lithologies to those in the Chongwe River (Fig. 3h) but additionally contains strongly metasomatized rocks that have been metamorphosed to whiteschist (high-pressure talc–kyanite assemblages) during the Neoproterozoic Zambezi Orogeny (John *et al.*, 2004). All lithologies in this river section have been intensely folded into millimeter and decimeter-scale sheath-folds (Fig. 3d). In the lower-strain hinge zones of these folds, many primary igneous textures and features have been preserved including discrete tuffaceous layers and lenses (e.g. GR 0755541–8268374–sample C7; Fig. 3e). Importantly, at GR 0755536–8268404 a strongly foliated quartz–feldspar–biotite–garnet leucogneiss (sample C9a) hosts 1–20 cm thick, foliation-parallel garnet-amphibolite layers (sample C9b). In the lower-strain regions the amphibolite is observed to cross-cut the dominant felsic gneiss foliation and crude layering (Fig. 3f), demonstrating that some of the amphibolites were once dykes. Rarely, these dykes retain texturally preserved chilled margins. The Chowe River section also contains up to 100 m thick lenses of mylonitized K-feldspar augen gneiss (Fig. 3g). At GR 0755513–8268419 (sample C10) tabular K-feldspar

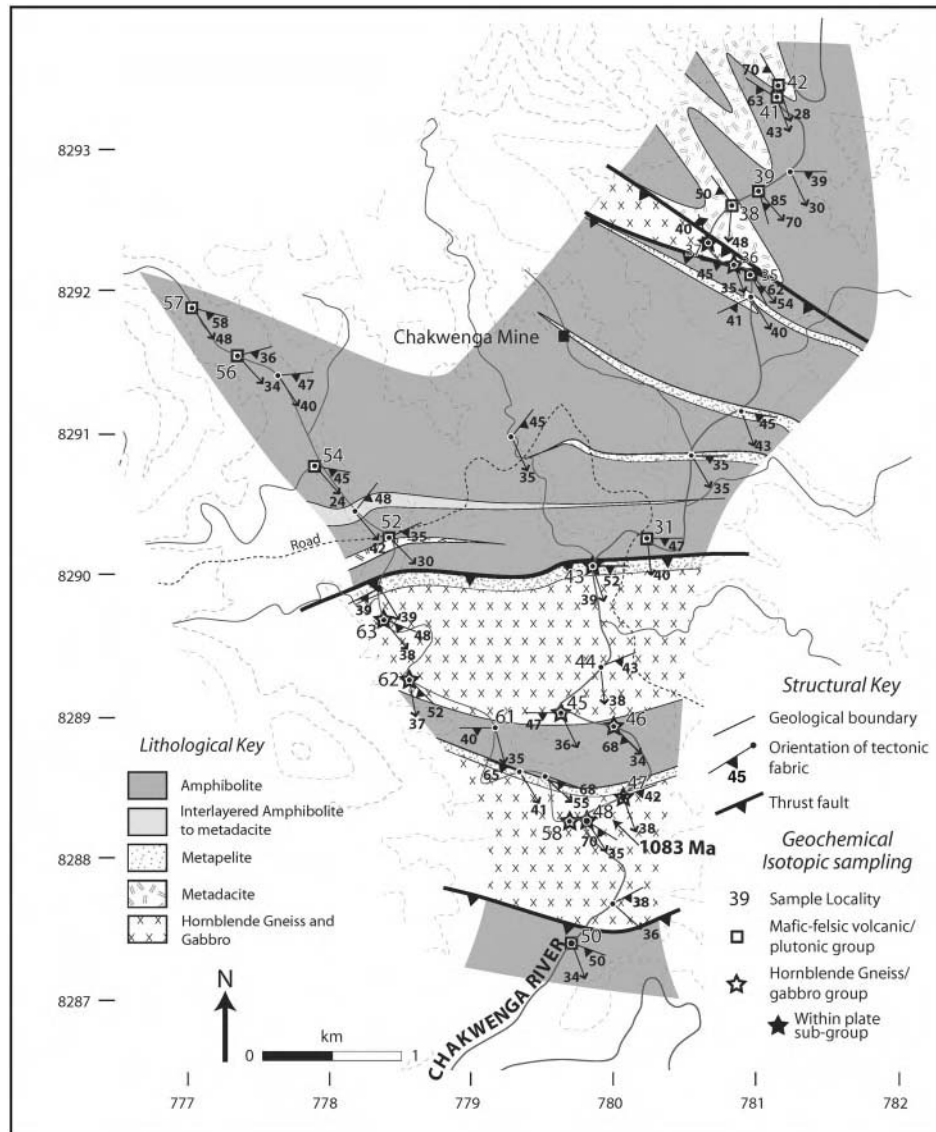


Fig. 2. Geological map of part of the Chakwenga Complex produced by S. Johnson and B. De Waele in 2004 (for location see Fig. 1c). The southerly part of the area is composed of coarse-grained (plutonic) hornblende gneiss and metagabbro, whereas the northern part is composed of extrusive, fine-grained meta-mafic to meta-felsic lithologies. The predominant tectonic fabric, including the thrust faults and folds, is Pan-African in age, and has completely modified the original distribution of the Mesoproterozoic igneous lithologies. UTM coordinates are the same as in Fig. 1c.

augen ~10 cm by 5 cm dominate a matrix composed of quartz and feldspar with minor biotite and muscovite. These augen are intensely deformed and in places the gneiss contains centimeter-scale layers and bands dominated by very fine-grained ultramylonitized K-feldspar augen. The margins of the augen gneiss bodies are intensely mylonitized, indicating that these units represent imbricate thrust lenses.

Because the whiteschist lithologies have undergone such intense metasomatic alteration (Johnson & Oliver 2002; John *et al.*, 2004) it is almost impossible to determine their

parental, pre-metasomatic geochemical composition and so they are not considered further here.

ANALYTICAL TECHNIQUES

Whole-rock major- and trace-element analyses

All samples were prepared and analysed by conventional X-ray fluorescence spectrometry (XRF) using the procedure and instrumentation described in Tani *et al.* (2005). Fresh samples were cut into slabs with a diamond-blade

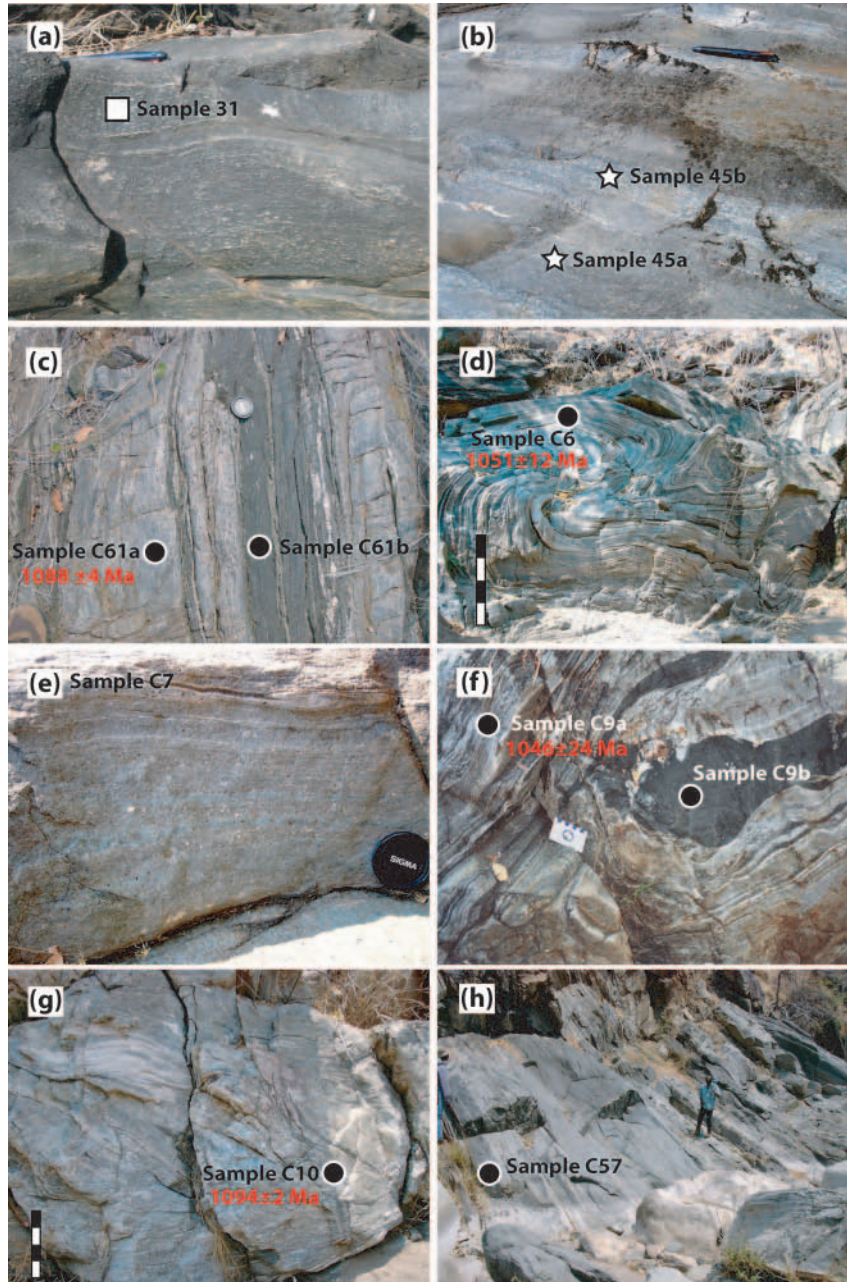


Fig. 3. Field photographs of the principal meta-mafic to meta-felsic igneous units in the Chakwenga and Chongwe complexes. (a) Chakwenga Complex: moderately deformed, meta-basaltic unit (sample 31). (b) Chakwenga Complex: typical example of the lithologies from the plutonic portion of the Chakwenga Complex. Sample 45a is a hornblende gneiss and sample 45b is a coarse-grained metagabbro, possibly a former gabbroic dyke. (c) Chongwe Complex: layered garnet-bearing meta-felsic and meta-mafic lithologies along the Chongwe River. The meta-felsic unit (sample C61a) has been dated by the SHRIMP U–Pb zircon technique (this study) at 1088 ± 4 Ma (Table 2). The meta-mafic material possibly represents former dykes. (d) Chongwe Complex: layered meta-mafic gneiss from the Chowe (Chiawa) River. Scale bar is 1 m in height. The unit has been folded into a sheath fold so that fold hinges and stretching lineations are parallel. The unit (sample C6) has been dated by the SHRIMP U–Pb zircon technique (this study) at 1051 ± 12 Ma (Table 2). (e) Chongwe Complex: meta-tuffaceous layer some 5 m structurally above sample C6 (Fig. 3d), indicating the extrusive nature of some lithologies. (f) Chongwe Complex: interlayered meta-mafic and meta-felsic gneiss from the Chowe River. In this lower-strain zone the meta-mafic unit is, in places, discordant to the layering or foliation of the felsic gneisses, indicating that some of these meta-mafic units represent former dykes that have subsequently been rotated into parallelism with the dominant Pan-African tectonic fabric. The felsic gneiss (sample C9a) has been dated using the SHRIMP U–Pb zircon technique (this study) at 1046 ± 26 Ma (Table 2). (g) Chongwe Complex: intensely deformed K-feldspar augen gneiss. Scale bar is 2 m in height. This unit occurs as a thrust-bound lens within the mafic to felsic gneisses of the Chowe River. The sample (C10) has been dated using the SHRIMP U–Pb zircon technique (this study) at 1094 ± 2 Ma (Table 2). (h) Chongwe Complex: a broad-scale view of the various mafic to felsic gneisses along the Chowe River. These units have compositions that range from meta-basalt to meta-andesite.

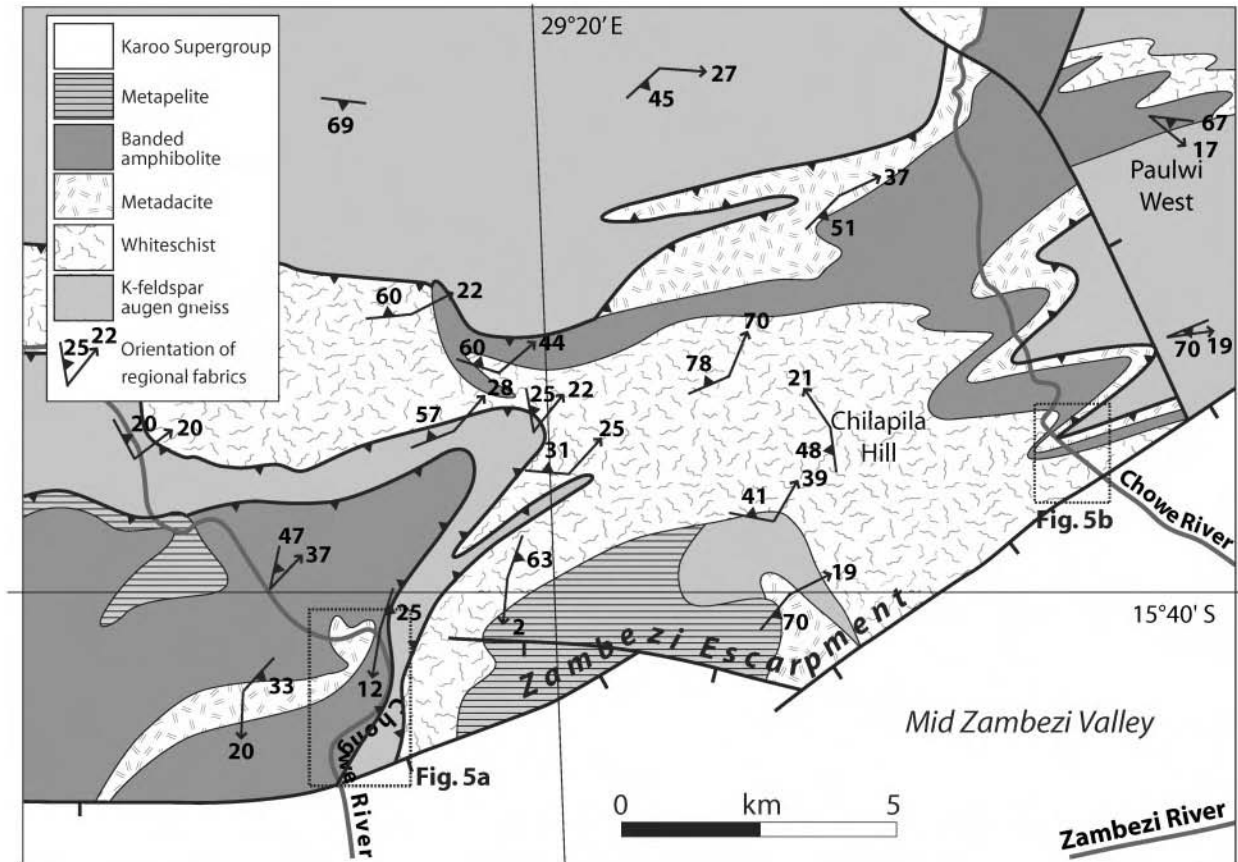


Fig. 4. Simplified geological map of the Chongwe Complex after the 1:250 000 Geological Survey of Zambia map series (Sheet No. SD-35-16; Barr, 1998). Dashed boxes show the location of the two rivers mapped in Fig. 5a and b. The structural symbols are the same as those in Fig. 2.

saw and the altered surfaces removed. The slab faces were polished and rinsed in an ultrasonic bath to remove any iron introduced by the diamond blade saw, before being coarsely crushed and washed in distilled water and acetone. The dried samples were crushed in a mortar and then powdered using an oscillatory alumina mill. Major- and trace-elements were analysed on glass beads and pressed powder pellets, respectively, using a RIGAKU SIMULTIX12 for major elements and a RIGAKU RIX3000 for trace elements. Instrumental procedures, standards, analytical conditions and detection limits have been outlined in detail by Tani *et al.* (2005). The major, trace and REE data were plotted using GDCKIT v2.2.1 (Janousek *et al.*, 2006). Numerical data are presented in Table 1.

Sensitive high-resolution ion-microprobe U–Pb zircon dating

Fresh rocks samples were crushed and heavy mineral separates obtained through conventional panning and high-density liquid separation in an ultra-clean environment. Zircon grains were picked under a binocular microscope and mounted alongside the CZ3 and/or FCI standard

zircon in an epoxy cast, which was polished to expose the grains mid-section. The mount was first imaged using an optical microscope, then coated with a thin layer of carbon and imaged on a JEOL 6400 electron microscope fitted with a cathodoluminescence (CL) detector. Operating conditions for CL imaging were 15 keV accelerating voltage, 5 nA current and a working distance of 16–25 mm. The mount was then repolished and thoroughly cleaned to minimize contamination (Pb), and then coated with a thin layer of Au to provide conductivity during the SHRIMP II analyses. The mount was loaded into the sample lock 24 h prior to analysis and pumped to high vacuum to allow outgassing, thereby minimizing hydride interference during the analysis. The analyses were conducted in two separate sessions, the first (Session A in Table 2) at the John de Laeter Centre for Mass Spectrometry (Curtin University of Technology) and the second (Session B in Table 2) at the National Institute for Polar Research (NIPR) in Tokyo. Operating procedures for the SHRIMP followed that described by Nelson (1996). In session A (Curtin University SHRIMP II), the primary beam intensity was ~2 nA with a slightly elliptical spot

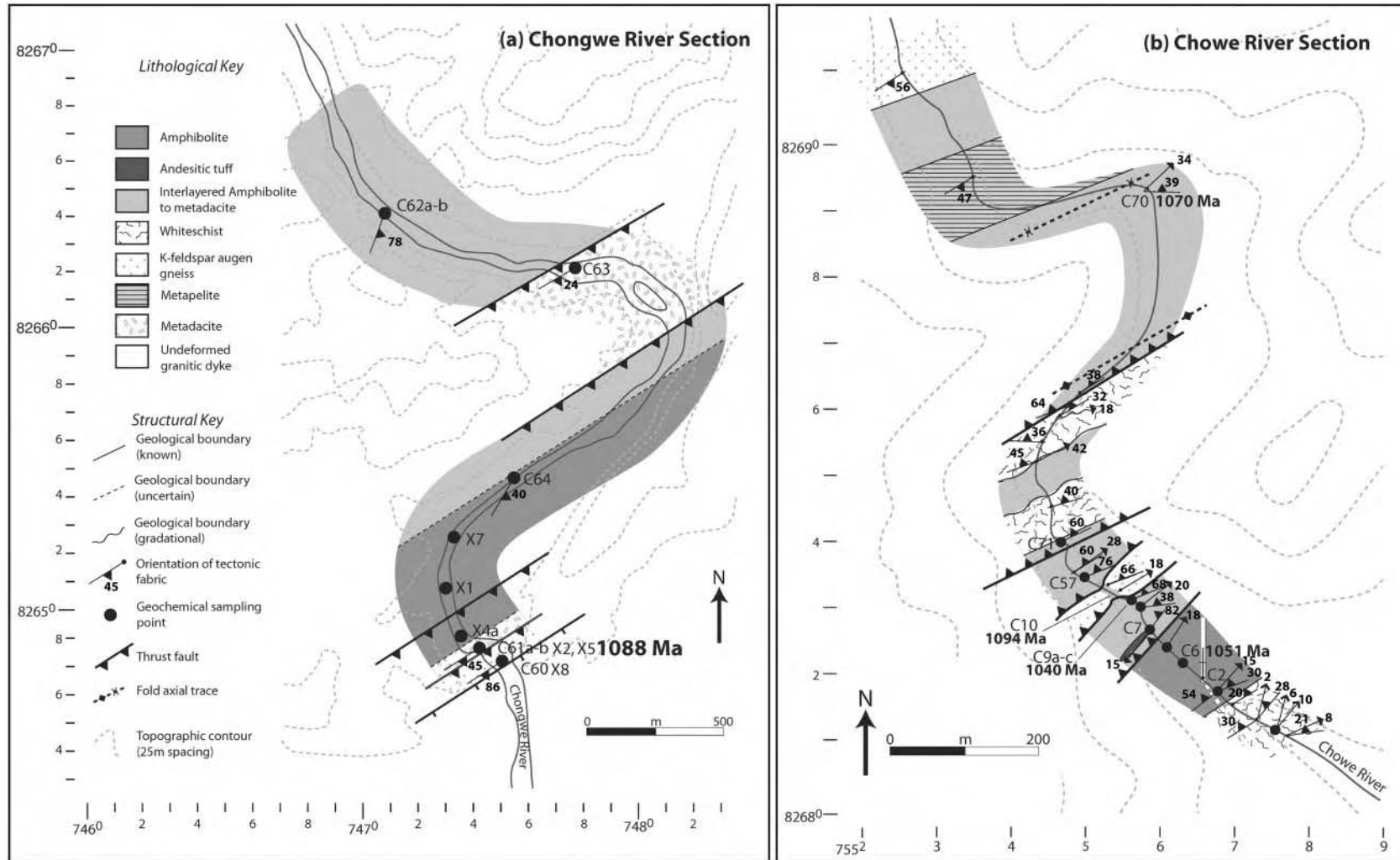


Fig. 5. Geological sections through the (a) Chongwe and (b) Chowe (Chiawa) rivers, compiled by the principal authors during various field seasons between 1999 and 2005. The dominant tectonic fabrics, folds and thrusts are Pan-African in age and, because of regional-scale sheath folding, repeats in lithologies could be the result of folding. Because many lithologies in the Chowe River section have been intensely altered by metasomatic activity (to whiteschists) during the Pan-African Zambezi Orogeny (John *et al.* 2004; Johnson *et al.*, 2005) the geochemistry of these altered rocks has not been considered here. Structural symbols are the same as those in Fig. 2

size of 30 μm , whereas at NIPR (SHRIMP II) the primary beam intensity was 4.4 nA with an elliptical spot size of 30 μm . Analyses of unknown zircon were interspersed with analyses on the standard zircon (CZ3 at Curtin University or FCl at NIPR) at a ratio of 3:1 to allow calibration of the $^{206}\text{Pb}/^{238}\text{U}$ ratio. In the case of standard FCl (which has variable U concentrations), two analyses of zircon standard SL13 (with a uniform U concentration of 238 ppm) were conducted to calculate the U concentration for the unknown analyses. Corrected ratios were calculated using SQUID software (Ludwig, 2001b), and calculation of pooled ages and plotting were done using ISOPLOT (Ludwig, 2001a). All data in Table 2 are reported at the 1σ confidence level. Age data for single zircons are reported in the text at the 1σ confidence level whereas the pooled ages (concordia ages, weighted mean $^{207}\text{Pb}/^{206}\text{Pb}$ or $^{206}\text{Pb}/^{238}\text{U}$ and lower or upper intercept ages) are reported at the 95% confidence level.

Whole-rock Sm–Nd isotopic analyses

Sr and Nd isotope ratios were determined by thermal ionization mass spectrometry (TIMS) at the Department of Geology and Geophysics at the University of Adelaide on a Finnigan MAT 262 system in static mode. All ground samples were leached in 3N HCl for 30 min at *c.* 100°C. The supernatant liquid was pipetted off, the sample washed in deionized water and the water pipetted off. The residue was then analysed for its isotopic composition. The long-term average for the in-house Nd standard (J&M specpure Nd₂O₃) is 0.511603 ± 9 (1σ of total population, $n=105$). The LaJolla standard gave 0.511828 ± 11 ($n=9$) and BCR-1 was 0.512593 ± 16 ($n=12$). Typical blanks are in the order of 100–200 pg for Nd. The average for the NBS987 Sr standard is 0.710258 ± 18 ($n=56$). Typical Sr blanks are better than 1.5 ng, which is negligible compared with a typical sample size of 10–100 mg of Sr. Initial ratios and model ages were calculated using the present-day Chondritic Uniform Reservoir (CHUR) of Goldstein *et al.* (1984) (0.512638).

In situ zircon Lu–Hf isotopic analyses

In situ analyses of the Lu–Hf ratio of the inherited zircon were performed on a multi-collector (MC) laser ablation inductively coupled plasma mass spectrometry (LA-MC-ICPMS) system at the Department of Earth and Planetary Sciences, Tokyo Institute of Technology, using the procedures documented by Iizuka & Hirata (2005). Analyses were carried out with a beam diameter of 62 μm , 3–10 Hz repetition rates and 15 s ablation times. All analyses were collected in a single session. Mass discrimination effects were corrected by normalizing to $^{179}\text{Hf}/^{177}\text{Hf} = 0.7325$ (Patchette *et al.*, 1981) for Hf and Lu, and to $^{173}\text{Yb}/^{171}\text{Yb} = 1.12346$ (Thirlwall and Anczkiewicz, 2004) for Yb using an exponential law. For the calculation

of initial Hf isotope ratio, the decay constant for ^{176}Lu proposed by Scherer *et al.* (2001) ($1.865 \times 10^{-11} \text{ year}^{-1}$) was used.

MAJOR, TRACE AND REE GEOCHEMISTRY

Bearing in mind that the rocks in this study have been metamorphosed to at least the mid-amphibolite facies, it is inappropriate to use fluid-mobile elements such as the alkali oxides CaO, Na₂O and K₂O and trace elements such as Rb, Sr, Ba for discussing tectonic environments or fractionation–assimilation pathways (Humphris & Thompson, 1978; Brekke *et al.*, 1988; Brouxel & Lapierre, 1988) and so we focus on the relatively immobile elements such as Zr, Y, Th and Nb, which are frequently used to distinguish the tectonomagmatic environment (e.g. Pearce & Norry, 1979; Meschede, 1986) of basaltic lithologies from low- to high-grade metamorphic terranes. The data for both the Chakwenga (open squares and stars) and Chongwe complexes (closed circles) (Table 1) are shown in a series of Harker variation (Fig. 6) and normalized trace-element and REE diagrams (Fig. 7), to discriminate the tectonic setting of these rocks.

Major- and trace-element data

The rocks in the Chakwenga and Chongwe complexes comprise a compositionally variable suite ranging from sub-alkaline basalt through to rhyodacite–rhyolite (Fig. 6a; Table 1). In general, the metabasalts of all groups have low Zr (<100 ppm), Y (<30 ppm), Th (<10 ppm) and Nb (<20 ppm) concentrations and high FeO (>10 wt %), TiO₂ (>1 wt %) and MgO (>5 wt %) contents (Table 1; Fig. 6b–h). With increasing silica content, FeO, TiO₂ and MgO progressively decrease and Zr, Y, Th and Nb progressively increase (Table 1; Fig. 6b–h). However, the Chakwenga hornblende gneisses and metagabbros have significantly higher Zr, Th and Nb contents at all SiO₂ concentrations, and have less well-constrained relationships than the mafic–felsic volcanic suites of both the Chakwenga and Chongwe complexes. The compositions and trends of the Chakwenga and Chongwe metavolcanic suites are similar to those of the Chewore Complex (Johnson & Oliver, 2000, 2004), where they were interpreted to represent a low-K tholeiitic suite that had undergone simple, closed-system fractionation.

In the normal mid-ocean ridge basalt (N-MORB)-normalized trace-element diagrams (Fig. 7a–c; normalization after Pearce, 1983), the metamafic lithologies from both the Chakwenga and Chongwe complexes display relatively flat profiles from Nb to Yb with element concentrations between 0.5 and 5 times that of N-MORB, and have relatively elevated (1.5–70 times) Th concentrations. All of the Chakwenga hornblende gneisses and meta-gabbros have much higher trace-element concentrations and plot with a positive sloping trace-element pattern.

Table 1: Whole-rock, major- and trace-element, and REE data for the Chakwenga, Chongwe and Chewore complexes

Chakwenga Complex																								
North of UTM 8290												South of UTM 8290												
Meta-basalt				Meta-basaltic andesite & andesite				Meta-dacite & rhyodacite				Gabbro and meta-basalt				Meta-diorite				Meta-granodiorite				
Sample:	35	41	39	31	50	61	54	57	43A	52	56	63	46	45B	37B	37A	47B	36	58	45A	62	48A	38	42
SiO ₂	44.75	46.40	47.12	48.32	48.94	50.05	51.89	53.97	63.19	65.41	67.52	42.46	46.93	50.93	51.03	51.28	52.35	55.17	59.64	61.44	67.24	67.96	75.00	76.48
TiO ₂	1.52	1.66	1.59	1.37	1.08	3.03	1.49	2.01	0.69	0.91	0.55	4.75	2.96	1.12	3.36	2.39	2.77	2.66	1.03	1.01	1.20	0.93	0.40	0.66
Al ₂ O ₃	15.63	14.02	14.26	14.69	13.70	11.38	13.72	13.43	11.09	14.36	15.01	13.80	12.00	14.53	13.25	18.62	11.49	13.55	16.20	17.98	14.08	12.54	13.53	10.34
Fe ₂ O ₃	15.09	16.29	14.86	15.21	12.71	21.63	13.28	12.02	6.97	8.21	6.55	23.17	20.61	12.91	15.91	10.90	19.43	12.89	10.19	9.10	4.91	6.66	2.95	4.82
MnO	0.23	0.25	0.18	0.23	0.20	0.29	0.19	0.15	0.46	0.10	0.04	0.22	0.31	0.19	0.18	0.13	0.32	0.15	0.18	0.05	0.04	0.15	0.03	0.07
MgO	9.87	7.45	8.67	8.19	8.24	2.44	7.06	6.44	3.15	2.98	0.69	4.79	4.67	8.81	3.76	2.28	1.97	3.54	4.47	3.07	2.43	1.30	0.45	1.42
CaO	8.18	9.41	9.49	8.84	11.96	7.61	8.74	9.79	11.95	2.29	1.92	7.37	8.93	7.82	7.32	9.36	7.53	8.35	2.67	0.69	4.39	9.19	0.82	3.42
Na ₂ O	3.53	2.88	3.60	2.97	1.98	2.34	3.16	1.84	0.22	2.33	6.91	2.78	2.66	3.68	1.86	3.70	2.58	1.65	2.93	1.08	2.96	0.75	4.26	2.01
K ₂ O	0.11	0.94	0.06	0.10	0.38	0.76	0.08	0.28	0.05	3.13	0.74	0.35	0.46	0.08	2.38	1.01	1.00	1.50	2.65	4.49	1.90	0.45	2.15	0.93
P ₂ O ₅	0.18	0.25	0.15	0.12	0.08	0.56	0.19	0.22	0.18	0.17	0.14	0.55	0.41	0.12	0.45	0.35	0.81	0.30	0.18	0.16	0.25	0.14	0.10	0.11
LOI	0.45	0.01	0.00	0.00	0.35	0.00	0.01	0.00	1.71	0.01	0.00	0.00	0.00	0.00	0.15	0.00	0.00	0.00	0.00	0.45	0.21	0.00	0.00	0.00
Total	99.52	99.56	99.97	100.05	99.62	100.08	99.81	100.15	99.67	99.89	100.06	100.22	99.94	100.17	99.64	100.01	100.25	99.75	100.10	99.50	99.61	100.07	99.69	100.26
Ba	34.1	774.5	14.2	170.2	59.8	144.3	20.7	50.8	40.4	904.8	108.9	122.2	88.2	47.1	806.4	542.6	287.9	458.3	808.3	811.1	407.8	106.8	767.9	206.4
Ni	182.7	128.2	189.0	109.2	90.1	15.8	126.6	115.1	28.5	54.0	<1.4	51.5	47.2	97.9	62.9	34.6	15.8	49.4	69.2	51.4	16.4	23.2	<1.4	24.4
Cu	6.6	3.8	17.1	65.8	30.3	136.6	0.5	140.4	22.5	10.2	23.2	40.7	200.5	8.8	79.5	32.2	37.2	136.5	56.0	105.3	0.5	1.3	184.4	2.8
Zn	142.9	259.3	99.8	100.5	80.8	181.8	88.8	88.0	39.0	63.6	22.9	144.7	164.2	85.2	141.6	83.2	142.5	107.2	95.0	79.0	20.5	35.4	42.3	36.1
Pb	7.1	1.9	10.3	3.4	6.2	12.1	1.1	2.0	3.6	9.7	2.8	22.4	1.5	6.7	11.2	11.5	6.5	6.4	17.3	13.4	1.4	25.0	2.7	6.0
Th	1.4	2.8	0.6	0.3	0.9	6.6	1.6	3.3	17.5	16.7	10.9	4.1	4.8	3.6	10.0	7.6	7.4	9.1	17.2	18.1	27.5	19.0	33.1	14.4
Rb	3.8	21.4	1.9	2.9	25.0	14.8	1.9	2.6	3.0	154.4	52.1	16.0	6.7	2.2	78.6	31.5	26.1	41.2	102.3	190.8	106.0	27.0	67.3	59.4
Sr	218.8	145.2	256.8	166.1	137.2	133.3	245.1	255.4	107.7	98.2	127.1	513.8	169.9	231.6	282.2	486.3	197.1	265.8	99.0	72.1	268.2	241.8	216.5	212.3
Y	22.5	22.9	18.9	19.7	17.0	61.2	22.2	17.7	33.9	27.1	78.6	56.0	45.2	19.2	37.3	27.9	75.9	34.1	33.6	33.8	52.6	41.1	91.2	25.0
Zr	67.1	70.7	54.0	51.9	41.8	215.9	80.5	118.2	189.3	214.5	509.0	235.6	144.5	74.7	294.4	214.3	251.7	251.0	203.5	196.6	242.9	206.2	464.6	188.2

(continued)

Table 1: Continued

Chakwenga Complex																								
North of UTM 8290												South of UTM 8290												
Sample:	Meta-basalt							Meta-basaltic andesite & andesite		Meta-dacite & rhyodacite			Gabbro and meta-basalt				Meta-diorite			Meta-granodiorite				
	35	41	39	31	50	61	54	57	43A	52	56	63	46	45B	37B	37A	47B	36	58	45A	62	48A	38	42
Nb	6.3	11.2	9.0	3.9	3.9	29.6	7.1	11.5	16.1	15.5	52.7	21.0	20.5	4.9	30.0	21.0	34.9	29.9	15.8	17.5	20.2	19.6	61.5	11.8
Hf	1.2	n/a	n/a	0.5	n/a	2.7	0.5	n/a	n/a	n/a	n/a	n/a	3.7	n/a	1.1	n/a	n/a	n/a	n/a	n/a	n/a	n/a	n/a	n/a
U	0.3	n/a	n/a	0.1	n/a	0.5	0.2	n/a	n/a	n/a	n/a	n/a	1.1	n/a	2.4	n/a	n/a	n/a	n/a	n/a	n/a	n/a	n/a	n/a
Sc	36.3	n/a	n/a	41.4	n/a	39.4	31.5	n/a	n/a	n/a	n/a	n/a	35.1	n/a	27.1	n/a	n/a	n/a	n/a	n/a	n/a	n/a	n/a	n/a
La	6.16	n/a	n/a	5.50	n/a	25.50	8.33	n/a	n/a	n/a	n/a	n/a	19.42	n/a	46.13	n/a	n/a	n/a	n/a	n/a	n/a	n/a	n/a	n/a
Ce	15.45	n/a	n/a	12.37	n/a	31.80	19.12	n/a	n/a	n/a	n/a	n/a	44.24	n/a	100.21	n/a	n/a	n/a	n/a	n/a	n/a	n/a	n/a	n/a
Pr	2.16	n/a	n/a	1.77	n/a	7.43	2.55	n/a	n/a	n/a	n/a	n/a	5.82	n/a	12.38	n/a	n/a	n/a	n/a	n/a	n/a	n/a	n/a	n/a
Nd	10.67	n/a	n/a	8.54	n/a	33.31	11.87	n/a	n/a	n/a	n/a	n/a	26.03	n/a	51.15	n/a	n/a	n/a	n/a	n/a	n/a	n/a	n/a	n/a
Sm	3.12	n/a	n/a	2.54	n/a	8.92	3.35	n/a	n/a	n/a	n/a	n/a	7.15	n/a	10.77	n/a	n/a	n/a	n/a	n/a	n/a	n/a	n/a	n/a
Eu	1.16	n/a	n/a	0.93	n/a	2.56	1.24	n/a	n/a	n/a	n/a	n/a	2.09	n/a	2.74	n/a	n/a	n/a	n/a	n/a	n/a	n/a	n/a	n/a
Gd	3.88	n/a	n/a	3.30	n/a	10.68	4.09	n/a	n/a	n/a	n/a	n/a	8.57	n/a	10.29	n/a	n/a	n/a	n/a	n/a	n/a	n/a	n/a	n/a
Tb	0.69	n/a	n/a	0.59	n/a	1.89	0.71	n/a	n/a	n/a	n/a	n/a	1.47	n/a	1.50	n/a	n/a	n/a	n/a	n/a	n/a	n/a	n/a	n/a
Dy	4.44	n/a	n/a	3.90	n/a	12.53	4.41	n/a	n/a	n/a	n/a	n/a	9.43	n/a	8.45	n/a	n/a	n/a	n/a	n/a	n/a	n/a	n/a	n/a
Ho	0.94	n/a	n/a	0.83	n/a	2.69	0.93	n/a	n/a	n/a	n/a	n/a	2.00	n/a	1.63	n/a	n/a	n/a	n/a	n/a	n/a	n/a	n/a	n/a
Er	2.72	n/a	n/a	2.39	n/a	7.99	2.65	n/a	n/a	n/a	n/a	n/a	5.73	n/a	4.43	n/a	n/a	n/a	n/a	n/a	n/a	n/a	n/a	n/a
Tm	0.39	n/a	n/a	0.34	n/a	1.17	0.38	n/a	n/a	n/a	n/a	n/a	0.84	n/a	0.60	n/a	n/a	n/a	n/a	n/a	n/a	n/a	n/a	n/a
Yb	2.54	n/a	n/a	2.22	n/a	7.59	2.37	n/a	n/a	n/a	n/a	n/a	5.36	n/a	3.69	n/a	n/a	n/a	n/a	n/a	n/a	n/a	n/a	n/a
Lu	0.38	n/a	n/a	0.32	n/a	1.12	0.35	n/a	n/a	n/a	n/a	n/a	0.80	n/a	0.50	n/a	n/a	n/a	n/a	n/a	n/a	n/a	n/a	n/a

(continued)

Table 1: *Continued*

Chongwe Complex																									
Meta-basalt												Meta-basaltic andesite and andesite					Meta-dacite and rhyolite								
C64	XCH6b	XCH4-3	X7	X1	X4a	XCH4-1	C62A	C9b	C57A	C2	C6	C61B	XCHI-2	C7	C9c	XCH4-4	C62B	X2	X5	C71	C61A	C63	C60	C9a	
SiO ₂	45.87	45.92	46.18	46.19	47.44	47.70	47.77	49.49	49.84	52.02	52.40	52.94	53.16	54.15	55.35	58.91	59.27	68.72	69.70	71.95	72.41	72.46	73.04	77.39	80.35
TiO ₂	3.06	2.08	1.41	0.53	1.28	2.53	1.38	2.14	2.93	1.82	2.18	2.47	2.06	1.76	0.99	1.92	1.27	0.82	0.67	0.48	0.88	0.59	0.50	0.08	0.90
Al ₂ O ₃	12.70	14.32	13.88	19.98	13.96	12.42	13.54	13.10	12.87	14.67	13.99	13.32	11.35	14.58	15.93	14.58	12.71	13.35	11.78	12.81	14.26	11.92	12.67	12.67	6.92
Fe ₂ O ₃	18.60	12.94	13.97	7.20	13.01	17.14	13.82	16.44	14.87	14.12	12.95	17.19	20.85	11.86	8.66	8.55	8.04	6.11	6.00	4.27	2.16	6.01	4.34	1.13	4.87
MnO	0.23	0.04	0.17	0.07	0.14	0.16	0.14	0.32	0.15	0.13	0.08	0.25	0.31	0.09	0.03	0.10	0.01	0.10	0.08	0.05	0.01	0.14	0.06	0.01	0.06
MgO	5.68	14.28	6.83	5.51	6.94	4.63	6.20	5.66	6.19	5.85	5.59	2.57	1.45	4.40	10.32	3.38	11.33	2.56	0.52	0.39	1.38	0.44	0.38	0.00	2.25
CaO	10.96	2.15	12.21	13.58	12.80	9.88	11.72	10.16	9.90	7.65	8.48	6.26	7.28	9.02	1.57	7.51	0.12	3.69	2.89	2.14	3.47	3.77	1.86	0.41	3.18
Na ₂ O	1.68	0.55	1.89	2.52	2.50	2.21	2.12	1.10	1.05	2.25	2.51	2.44	1.00	2.31	1.29	2.40	0.13	2.24	2.52	3.08	3.75	3.15	2.96	3.64	0.59
K ₂ O	0.67	1.03	0.88	1.31	1.26	0.66	1.13	0.77	0.86	0.50	0.93	2.13	1.31	1.06	1.93	1.23	1.01	1.95	2.80	3.66	1.14	1.48	4.10	4.75	0.59
P ₂ O ₅	0.09	0.16	0.12	0.01	0.10	0.27	0.13	0.23	0.44	0.23	0.23	0.41	0.71	0.40	0.15	0.54	0.10	0.19	0.22	0.10	0.26	0.09	0.10	0.02	0.11
LOI	0.01	6.10	2.10	2.64	0.67	1.94	1.79	0.15	0.52	0.47	0.24	0.01	0.15	0.67	3.82	0.51	5.50	0.03	2.56	0.62	0.00	0.00	0.00	0.00	0.01
Total	99.54	99.57	99.64	99.54	100.10	99.54	99.74	99.57	99.60	99.71	99.56	99.99	99.62	100.30	100.04	99.63	99.49	99.76	99.74	99.55	99.72	100.04	100.01	100.11	99.83
Ba	112.6	94.5	154.5	203.0	185.5	132.0	85.0	91.9	117.7	30.5	91.1	699.4	387.8	235.0	253.7	281.0	115.0	465.1	811.0	756.0	299.1	596.1	728.3	82.0	151.1
Ni	67.1	155.0	85.0	80.0	80.0	35.0	60.0	68.0	79.9	72.1	68.9	13.6	10.5	45.0	106.2	47.2	80.0	60.8	10.0	15.0	21.1	<1.4	<1.4	<1.4	26.6
Cu	234.3	30.0	125.0	130.0	195.0	165.0	70.0	240.1	48.5	0.6	3.9	37.3	89.3	55.0	6.8	13.7	20.0	12.3	50.0	65.0	59.4	7.5	19.1	<1.3	17.9
Zn	114.6	<12.7	100.0	45.0	65.0	115.0	45.0	115.3	69.4	26.2	13.5	149.6	223.0	50.0	<12.7	32.4	<12.7	50.8	75.0	75.0	<12.7	70.9	67.6	79.7	29.2
Pb	4.5	0.0	10.0	5.0	5.0	5.0	0.0	3.3	1.4	2.2	4.4	11.4	9.8	0.0	2.7	3.3	0.0	7.2	20.0	40.0	6.9	20.9	27.8	23.2	4.6
Th	1.9	0.0	0.0	0.0	0.0	0.0	0.0	2.1	3.3	6.0	6.3	7.8	5.3	1.0	7.9	2.1	5.0	13.2	17.0	21.0	48.4	22.9	22.7	24.2	3.1
Rb	22.9	48.8	19.4	93.8	33.8	17.4	9.0	12.8	9.0	27.2	27.7	100.2	51.0	21.6	103.6	40.7	51.2	101.1	119.0	190.5	94.2	40.4	199.7	241.4	21.5
Sr	111.4	18.2	130.0	299.0	158.5	124.0	142.5	70.2	121.9	127.4	241.3	335.7	65.1	236.0	65.5	282.8	<18.8	307.9	137.5	82.1	170.5	166.4	89.1	<18.8	108.0
Y	18.2	21.5	18.5	9.5	19.5	39.0	22.0	28.2	37.0	32.4	35.8	50.3	77.6	33.5	23.9	41.0	30.0	29.7	70.0	68.5	70.7	81.5	57.1	137.8	15.6
Zr	59.4	110.0	40.0	17.0	45.0	112.0	52.5	88.1	148.3	141.3	170.2	208.2	399.4	147.0	118.1	354.5	137.0	261.9	352.0	320.0	272.9	546.4	343.4	174.0	183.1

(continued)

Table 1: Continued

Chongwe Complex																									
Meta-basalt												Meta-basaltic andesite and andesite					Meta-dacite and rhyolite								
C64	XCH6b	XCH4-3	X7	X1	X4a	XCH4-1	C62A	C9b	C57A	C2	C6	C61B	XCHI-2	C7	C9c	XCH4-4	C62B	X2	X5	C71	C61A	C63	C60	C9a	
Nb	3.5	11.0	3.0	3.0	5.0	17.0	4.0	6.7	13.3	10.0	8.6	24.9	23.7	14.0	9.7	30.0	10.0	10.9	27.0	29.0	27.0	34.0	25.6	64.6	7.0
Hf	1.0	4.0	1.0	0.0	1.0	4.0	1.0	1.0	3.5	n/a	n/a	3.5	n/a	4.0	0.8	n/a	5.0	n/a	12.0	11.0	n/a	n/a	n/a	n/a	n/a
U	0.6	1.5	0.0	0.0	0.0	0.5	0.0	0.5	0.4	n/a	n/a	1.5	n/a	0.5	0.6	n/a	0.5	n/a	6.0	6.0	n/a	n/a	n/a	n/a	n/a
Sc	42.7	n/a	n/a	n/a	n/a	n/a	n/a	40.2	36.8	n/a	n/a	34.6	n/a	n/a	21.3	n/a	n/a	n/a	n/a	n/a	n/a	n/a	n/a	n/a	n/a
La	7.98	n/a	4.50	n/a	5.00	13.00	6.50	8.29	18.15	n/a	n/a	27.77	n/a	21.00	33.94	n/a	29.00	n/a	54.00	53.00	n/a	n/a	n/a	55.50	n/a
Ce	18.30	n/a	10.00	n/a	12.50	30.50	14.50	20.26	46.17	n/a	n/a	60.66	n/a	45.00	66.25	n/a	72.00	n/a	117.50	114.00	n/a	n/a	n/a	120.00	n/a
Pr	2.37	n/a	1.70	n/a	1.80	4.30	2.10	2.85	6.79	n/a	n/a	7.62	n/a	5.60	7.24	n/a	9.10	n/a	14.30	13.40	n/a	n/a	n/a	15.10	n/a
Nd	10.73	n/a	8.50	n/a	8.50	19.50	11.00	13.74	32.26	n/a	n/a	32.77	n/a	23.50	26.95	n/a	37.00	n/a	58.50	52.00	n/a	n/a	n/a	61.50	n/a
Sm	2.94	n/a	2.50	n/a	2.60	5.80	2.90	4.02	7.74	n/a	n/a	8.31	n/a	5.30	5.14	n/a	6.70	n/a	12.10	11.80	n/a	n/a	n/a	16.50	n/a
Eu	1.15	n/a	1.10	n/a	1.00	2.00	1.10	1.44	2.44	n/a	n/a	2.27	n/a	1.60	1.14	n/a	1.80	n/a	3.00	1.80	n/a	n/a	n/a	2.20	n/a
Gd	3.56	n/a	3.20	n/a	3.20	7.10	3.40	4.95	7.75	n/a	n/a	9.62	n/a	6.00	4.76	n/a	7.00	n/a	13.40	11.40	n/a	n/a	n/a	18.90	n/a
Tb	0.62	n/a	0.70	n/a	0.60	1.20	0.70	0.86	1.22	n/a	n/a	1.65	n/a	1.10	0.63	n/a	1.10	n/a	2.30	2.10	n/a	n/a	n/a	3.80	n/a
Dy	3.91	n/a	3.80	n/a	3.50	7.00	4.10	5.62	7.61	n/a	n/a	10.52	n/a	6.10	3.19	n/a	5.50	n/a	12.70	11.90	n/a	n/a	n/a	22.10	n/a
Ho	0.81	n/a	0.70	n/a	0.80	1.40	0.90	1.20	1.58	n/a	n/a	2.23	n/a	1.30	0.56	n/a	1.10	n/a	2.60	2.40	n/a	n/a	n/a	5.00	n/a
Er	2.26	n/a	2.10	n/a	2.10	4.40	2.20	3.53	4.56	n/a	n/a	6.54	n/a	3.40	1.48	n/a	3.50	n/a	7.30	6.90	n/a	n/a	n/a	14.80	n/a
Tm	0.32	n/a	0.30	n/a	0.30	0.70	0.40	0.51	0.65	n/a	n/a	0.95	n/a	0.50	0.20	n/a	0.50	n/a	1.30	1.10	n/a	n/a	n/a	2.50	n/a
Yb	2.03	n/a	2.00	n/a	1.80	3.70	2.10	3.38	4.12	n/a	n/a	6.22	n/a	3.30	1.27	n/a	2.90	n/a	6.80	6.70	n/a	n/a	n/a	14.90	n/a
Lu	0.30	n/a	0.20	n/a	0.30	0.60	0.30	0.52	0.63	n/a	n/a	0.91	n/a	0.50	0.19	n/a	0.50	n/a	1.20	1.10	n/a	n/a	n/a	2.30	n/a

(continued)

Table 1: *Continued*

	Chewore Complex					Chewore Ophiolite
	Kaourera Arc					
	373	236	165	286	220a	
SiO ₂	42.49	48.51	49.7	49.73	66.14	47.48
TiO ₂	2.08	0.7	1.02	0.68	3	0.74
Al ₂ O ₃	14.19	16.75	15.17	15.2	15.92	17
Fe ₂ O ₃	18.98	11.13	11.81	10.78	1.96	10.93
MnO	0.3	0.19	0.25	0.21	0.05	0.24
MgO	8.84	8.55	7.47	8.64	0.22	8.47
CaO	10.48	10.87	10.19	9.7	3.05	8.65
Na ₂ O	1.83	2.58	2.68	3.39	8.35	2.51
K ₂ O	0.61	0.43	0.52	0.23	0.24	2.66
P ₂ O ₅	0.06	0.1	0.12	0.05	0.46	0.13
LOI	0.00	0.00	0.75	1.02	0.00	0.95
Total	99.86	99.81	99.68	99.63	99.39	99.76
Ba	33.0	1370.0	108.0	72.0	414.0	n/a
Ni	88.0	204.0	125.0	237.0	8.0	211.0
Cu	n/a	n/a	n/a	n/a	n/a	n/a
Zn	n/a	n/a	n/a	n/a	n/a	n/a
Pb	2.0	1.0	5.0	<1	3.0	n/a
Th	1.0	<1	2.0	1.0	14.0	n/a
Rb	23.0	17.0	10.0	2.0	6.0	n/a
Sr	67.0	172.0	216.0	296.0	61.0	n/a
Y	14.0	17.0	24.0	15.0	84.0	17.0
Zr	14.0	36.0	92.0	31.0	413.0	46.0
Nb	3.0	1.0	4.0	2.0	24.0	1.0
Hf	n/a	n/a	n/a	n/a	n/a	n/a
U	2.0	<2	<2	2.0	5.0	n/a
Sc	51.0	40.0	39.0	15.0	13.0	30.0
La	3.00	2.70	8.00	2.20	4.00	4.40
Ce	9.00	5.90	27.00	5.90	24.00	9.90
Pr	n/a	0.70	n/a	1.00	n/a	1.40
Nd	n/a	4.40	n/a	4.40	n/a	7.00
Sm	n/a	1.40	n/a	1.10	n/a	1.90
Eu	n/a	0.70	n/a	0.40	n/a	0.90
Gd	n/a	2.00	n/a	2.10	n/a	2.40
Tb	n/a	N/A	n/a	N/A	n/a	n/a
Dy	n/a	2.80	n/a	2.60	n/a	3.00
Ho	n/a	0.60	n/a	0.60	n/a	0.60
Er	n/a	2.00	n/a	1.80	n/a	2.20
Tm	n/a	N/A	n/a	N/A	n/a	n/a
Yb	n/a	1.80	n/a	1.90	n/a	2.00
Lu	n/a	0.30	n/a	0.30	n/a	0.30

n/a, not available. LOI, loss on ignition.

Although there appears to be a clear distinction between the Chakwenga hornblende gneisses or metagabbros and the Chakwenga metabasalts, the latter overlap with metabasalts from the Chongwe Complex. None of the samples display relative negative Nb anomalies, a feature usually considered characteristic of supra-subduction-zone magmas. Two Chakwenga hornblende gneiss samples from the north of the mapping area (37a and 37b; closed stars; Fig. 2) have much steeper trace-element profiles that crosscut the patterns for the other Chakwenga meta-basaltic samples. Four Chewore Complex metabasalts are shown in Fig. 7c for comparison (see also Table 1). All these rocks have a similar, flat trace-element profiles to the bulk of the Chakwenga–Chongwe metabasalts but have relative, negative Nb anomalies.

In Fig. 8, the compositions of the meta-basalts are plotted on two of the most popular basalt tectonic discrimination diagrams, the 2Nb–Zr/4–Y triangular plot of Pearce & Norry (1979) and the Zr/Y–Zr binary plot of Meschede (1986). The data exhibit significant scatter, reflecting the variable Y, Zr and Nb concentrations as illustrated in the Harker variation diagrams (Fig. 6e, g and h). Data from the Chewore Complex plot within the N-MORB–volcanic arc basalt field in both diagrams, attesting to their relatively low and uniform Nb and Zr contents. The metabasalts of the Chakwenga and Chongwe complexes scatter within the N-MORB, enriched MORB (E-MORB), volcanic arc basalt and within-plate tholeiite fields (Fig. 8). Samples 37a and 37b from the Chakwenga Complex plot consistently within the within-plate basalt field in both diagrams. These two metabasalts have similar Zr, Nb and Y concentrations to the other metabasalts (Table 1 and Fig. 6) but their element ratios, especially Zr/Y (Fig. 6i), are appreciably different, suggesting that they may have a different tectonic setting from the other Chakwenga and Chongwe metabasalts.

REE data

REE data are tabulated in Table 1 and shown as chondrite-normalized REE plots in Fig. 7d–f (after Nakamura, 1974). The meta-basaltic lithologies from the Chakwenga and Chongwe complexes have gently sloping, parallel, light REE (LREE)-enriched patterns that become progressively more LREE-enriched with increasing REE content compared with chondrite (Fig. 7d and e). Again, the Chongwe metabasalts show a large compositional range and overlap with the Chakwenga hornblende gneisses and meta-gabbros. The less-evolved metabasalts (i.e. those with the lowest REE concentrations of 10–20 times chondrite) have average La/Sm_N and La/Yb_N ratios of 1.45 and 1.94 whereas the most enriched samples have REE concentrations 50–110 times that of chondrite with La/Sm_N and La/Yb_N ratios of 1.4 and 3.0. These enriched patterns are similar to those of the Chongwe felsic gneisses

Table 2: U–Pb SHRIMP data for zircon from meta-igneous lithologies in the Chewore–Rufunsa Terrane

Spot name	f ₂₀₆ (%)	U (ppm)	Th (ppm)	²³² Th/ ²³⁸ U	²³⁸ U/ ²⁰⁶ Pb 2σ% error	²⁰⁷ Pb/ ²⁰⁶ Pb 2σerror	²⁰⁶ Pb/ ²³⁸ U age 1σ abs error (Ma)	²⁰⁷ Pb/ ²⁰⁶ Pb age 1σ abs error (Ma)	Conc. (%)	Session
Chongwe Complex										
<i>Sample C6, banded mafic gneiss, Chowe River</i>										
c6-1r	0.07	1051	61	0.06	10.71924 ± 0.56908	0.05900 ± 0.57927	575 ± 3	567 ± 13	101	A
c6-2r	—	831	80	0.10	10.61574 ± 0.54851	0.05939 ± 0.51691	580 ± 3	581 ± 11	100	A
c6-3r	0.02	1121	86	0.08	10.69073 ± 0.46263	0.05879 ± 0.51805	576 ± 3	559 ± 11	103	A
c6-4r	0.15	719	73	0.10	10.65038 ± 0.47410	0.05874 ± 0.87636	579 ± 3	558 ± 19	104	A
c6-5r	0.02	1038	68	0.07	10.79746 ± 0.46669	0.05960 ± 0.54207	571 ± 3	589 ± 12	97	A
c6-6r	0.11	811	93	0.12	10.76238 ± 0.49128	0.05881 ± 0.78736	573 ± 3	560 ± 17	102	A
c6-1c	2.61	398	194	0.50	5.56142 ± 0.61764	0.07120 ± 4.51502	1066 ± 6	963 ± 92	110	A
c6-7c	0.19	408	243	0.62	5.72980 ± 0.71308	0.07404 ± 0.65987	1037 ± 7	1042 ± 13	99	A
c6-2c	0.08	286	149	0.54	5.62961 ± 0.52132	0.07427 ± 0.70332	1054 ± 5	1049 ± 14	101	A
c6-8c	0.07	571	322	0.58	5.79393 ± 0.62580	0.07462 ± 0.66200	1026 ± 6	1058 ± 13	97	A
c6-5c	0.08	572	335	0.60	5.53375 ± 0.49008	0.07445 ± 0.47005	1071 ± 5	1054 ± 9	102	A
<i>Sample C9, leucocratic gnt-bearing gneiss, Chowe River</i>										
c9-1r	—	52	3	0.06	10.89914 ± 1.99583	0.07070 ± 2.207183	566 ± 11	949 ± 45	60	A
c9-2r	—	75	20	0.27	10.71857 ± 1.90091	0.06785 ± 4.549956	575 ± 10	864 ± 94	67	A
c9-3r	0.21	24	29	1.24	10.38798 ± 2.39509	0.07208 ± 5.924726	592 ± 14	988 ± 121	60	A
c9-4r	0.01	253	28	0.11	6.12206 ± 1.65345	0.07579 ± 2.576515	975 ± 15	1089 ± 52	90	A
c9-1c	—	95	50	0.55	6.69910 ± 1.75814	0.07310 ± 1.261049	897 ± 15	1017 ± 26	88	A
c9-2c	0.00	483	28	0.06	5.94521 ± 1.86839	0.07391 ± 0.508414	1002 ± 17	1039 ± 10	96	A
c9-3c	0.02	84	91	1.11	5.46274 ± 1.76293	0.07946 ± 1.138151	1084 ± 18	1184 ± 22	92	A
c9-4c	—	92	60	0.68	2.58298 ± 2.01914	0.12867 ± 1.367012	2110 ± 36	2080 ± 24	101	A
<i>Sample C10, K-feldspar augen gneiss, Chowe River</i>										
c10-1	0.00	405	517	1.32	2.92006 ± 0.65761	0.11741 ± 0.29867	1898 ± 11	1917 ± 5	99	A
c10-2r	0.16	815	10	0.01	5.43830 ± 0.58466	0.07616 ± 0.48258	1088 ± 6	1099 ± 10	99	A
c10-3r	0.01	1819	7	0.00	5.40517 ± 0.43034	0.07558 ± 0.66673	1094 ± 4	1084 ± 13	101	A
c10-4r	0.00	864	8	0.01	5.40800 ± 0.62820	0.07612 ± 0.34033	1094 ± 6	1098 ± 7	100	A
c10-5r	0.47	980	7	0.01	5.03521 ± 0.47021	0.07345 ± 1.25832	1168 ± 5	1026 ± 25	112	A
c10-5c	0.02	352	281	0.83	3.16355 ± 1.20669	0.11062 ± 0.34983	1771 ± 19	1810 ± 6	98	A
c10-6r	0.06	618	5	0.01	5.35104 ± 0.52102	0.07576 ± 0.44300	1104 ± 5	1089 ± 9	101	A
c10-6c	0.06	289	298	1.07	2.98701 ± 0.60448	0.11880 ± 0.46144	1862 ± 10	1938 ± 8	96	A
c10-7r	0.02	502	5	0.01	5.25263 ± 0.50421	0.07638 ± 0.46518	1123 ± 5	1105 ± 9	102	A
c10-8r	0.21	721	10	0.01	5.43129 ± 0.48875	0.07507 ± 0.82559	1089 ± 5	1070 ± 17	102	A

(continued)

Table 2: Continued

Spot name	f206 (%)	U (ppm)	Th (ppm)	²³² Th/ ²³⁸ U	²³⁸ U/ ²⁰⁶ Pb 2σ% error	²⁰⁷ Pb/ ²⁰⁶ Pb 2σerror	²⁰⁶ Pb/ ²³⁸ U age 1σ abs error (Ma)	²⁰⁷ Pb/ ²⁰⁶ Pb age 1σ abs error (Ma)	Conc. (%)	Session
<i>Sample c61a, leucocratic gnt-bearing gneiss, Chongwe River</i>										
c61a-1	—	164	143	0.90	5.50631 ± 1.21631	0.07560 ± 1.02701	1076 ± 12	1085 ± 21	99	A
c61a-2	—	234	127	0.56	5.42873 ± 1.16843	0.07613 ± 0.84319	1090 ± 12	1098 ± 17	99	A
c61a-3	—	231	125	0.56	5.97770 ± 2.84125	0.07353 ± 0.85312	997 ± 26	1028 ± 17	97	A
c61a-4	—	296	179	0.62	5.45369 ± 1.12307	0.07585 ± 0.59803	1085 ± 11	1091 ± 12	99	A
c61a-5	—	307	194	0.65	5.35156 ± 1.12273	0.07571 ± 0.58574	1104 ± 11	1088 ± 12	102	A
c61a-6	0.11	162	87	0.56	5.25484 ± 1.19368	0.07545 ± 1.21765	1123 ± 12	1081 ± 24	104	A
c61a-7	0.07	153	64	0.43	6.36256 ± 1.35353	0.07222 ± 1.07619	941 ± 12	992 ± 22	95	A
c61a-8	—	205	117	0.59	5.69987 ± 1.31871	0.07596 ± 0.78398	1042 ± 13	1094 ± 16	95	A
c61a-9	0.01	204	128	0.65	5.46989 ± 1.27001	0.07582 ± 0.86112	1082 ± 13	1090 ± 17	99	A
c61a-10	0.04	118	92	0.80	5.44970 ± 1.62184	0.07480 ± 1.39443	1086 ± 16	1063 ± 28	102	A
c61a-11	—	304	140	0.48	6.74331 ± 1.26348	0.07215 ± 0.74239	891 ± 11	990 ± 15	89	A
c61a-12	0.13	300	218	0.75	5.59175 ± 1.16937	0.07522 ± 0.86784	1061 ± 11	1074 ± 17	99	A
<i>Sample c70, leucocratic gnt-bearing gneiss, Chowe River</i>										
c70-1	0.04	324	131	0.42	5.53845 ± 0.62363	0.07452 ± 0.75185	1070 ± 6	1056 ± 15	101	A
c70-1	0.02	114	97	0.88	5.49421 ± 1.02711	0.07542 ± 1.41919	1078 ± 10	1080 ± 28	100	A
c70-2	0.02	215	143	0.69	5.58110 ± 0.70582	0.07554 ± 1.18702	1062 ± 7	1083 ± 24	98	A
c70-3	0.05	328	206	0.65	5.52854 ± 0.62405	0.07493 ± 0.68403	1072 ± 6	1067 ± 14	100	A
c70-4	0.04	281	177	0.65	5.53400 ± 0.56566	0.07465 ± 0.76037	1071 ± 6	1059 ± 15	101	A
c70-5	—	231	112	0.50	5.50932 ± 0.61625	0.07521 ± 0.65633	1075 ± 6	1074 ± 13	100	A
Chakwenga Complex										
<i>Sample Chak48a, leucocratic gneiss, Chakwenga River</i>										
Chak48-1	0.20	108	70	0.67	5.70396 ± 3.39763	0.07511 ± 2.12388	1041 ± 33	1071 ± 43	97	B
Chak48-2C	0.24	124	81	0.68	5.43820 ± 5.19690	0.07468 ± 3.07806	1088 ± 52	1060 ± 62	103	B
Chak48-3	0.36	117	143	1.26	5.18053 ± 3.46294	0.07498 ± 1.64758	1138 ± 36	1068 ± 33	106	B
Chak48-4	0.67	254	128	0.52	4.32681 ± 2.74569	0.10520 ± 1.84928	1340 ± 33	1718 ± 34	78	B
Chak48-6	0.22	207	116	0.58	2.30720 ± 4.46117	0.13612 ± 2.41763	2321 ± 87	2178 ± 42	106	B
Chak48-7	0.22	115	55	0.49	2.89786 ± 3.60433	0.11557 ± 1.45084	1911 ± 59	1889 ± 26	101	B
Chak48-8	0.07	201	146	0.75	3.02288 ± 8.62870	0.12008 ± 2.12391	1842 ± 138	1957 ± 38	94	B
Chak48-10	0.23	103	156	1.56	6.52338 ± 4.22020	0.07379 ± 3.22021	919 ± 36	1036 ± 65	87	B
Chak48-11	0.81	68	54	0.38	2.88023 ± 4.80980	0.11877 ± 3.46707	1921 ± 80	1938 ± 62	99	B
Chak48-12	—	156	334	2.20	7.34102 ± 7.24250	0.07657 ± 2.09715	823 ± 56	1110 ± 42	65	B
Chak48-13	0.91	82	54	0.68	5.61269 ± 4.55764	0.07410 ± 3.51440	1057 ± 44	1044 ± 71	101	B
Chak48-14	1.19	109	65	0.61	5.92126 ± 5.31089	0.07412 ± 3.04954	1006 ± 49	1045 ± 62	96	B
Chak48-16	0.61	81	59	0.74	5.40447 ± 3.81865	0.07357 ± 2.69063	1094 ± 38	1030 ± 54	106	B
Chak48-17	0.18	388	204	0.54	5.47425 ± 3.25447	0.07670 ± 1.54649	1082 ± 32	1113 ± 31	97	B
Chak48-1.2	1.29	114	85	0.77	5.35585 ± 5.51282	0.07631 ± 5.57541	1104 ± 56	1103 ± 111	100	B

Session A: SHRIMP II, Curtin University; 30 μm spot, 2 nA and regressed to 30 analyses of in-house standard CZ3. Session B: SHRIMP II, National Institute for Polar Research, Tokyo; 30 μm spot size, 4.4 nA and regressed to 25 analyses of in-house standard FC1. The parameter f206 is the proportion of common ²⁰⁶Pb in the total ²⁰⁶Pb. All ratios and ages are corrected for common Pb using measured ²⁰⁴Pb and a composition appropriate to the age of the zircon (Stacey & Kramers, 1975). Conc. (%) is per cent concordant.

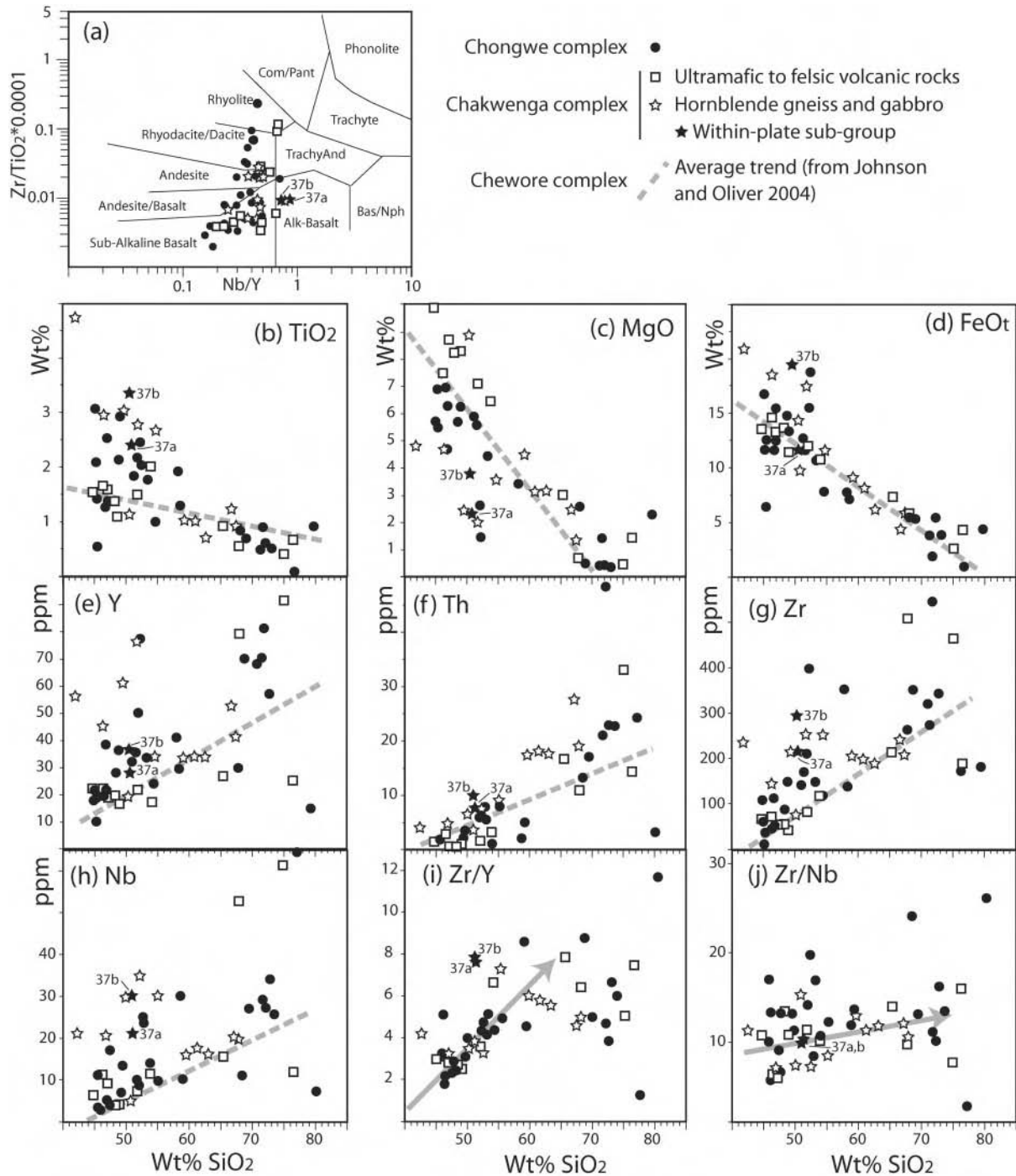


Fig. 6. Major- and trace-element data for the Chakwenga, Chongwe, and Chewore complexes (Table 1) plotted in a Zr/TiO₂ vs Nb/Y classification diagram (a) (Winchester & Floyd, 1977) and as a series of Harker diagrams (b-j). The fluid-mobile elements such as CaO, Na₂O, K₂O, Rb, Ba, Sr are not considered, as their concentrations will have been altered significantly during the Pan-African Zambezi Orogeny. Additional data for the Chewore Complex are from Johnson & Oliver (2000, 2004).

(stippled field in Fig. 7d; Table 1). Sample 37b has a much steeper REE profile that crosscuts the other Chakwenga metamafic rocks and has La/Sm_N and La/Yb_N ratios of 2.63 and 8.34, respectively. The three representative

samples from the Chewore Complex have lower REE concentrations than the Chongwe and Chakwenga samples and flat REE patterns with La/Sm_N and La/Yb_N ratios of 1.0 and 0.5 (Fig. 7f; Table 1).

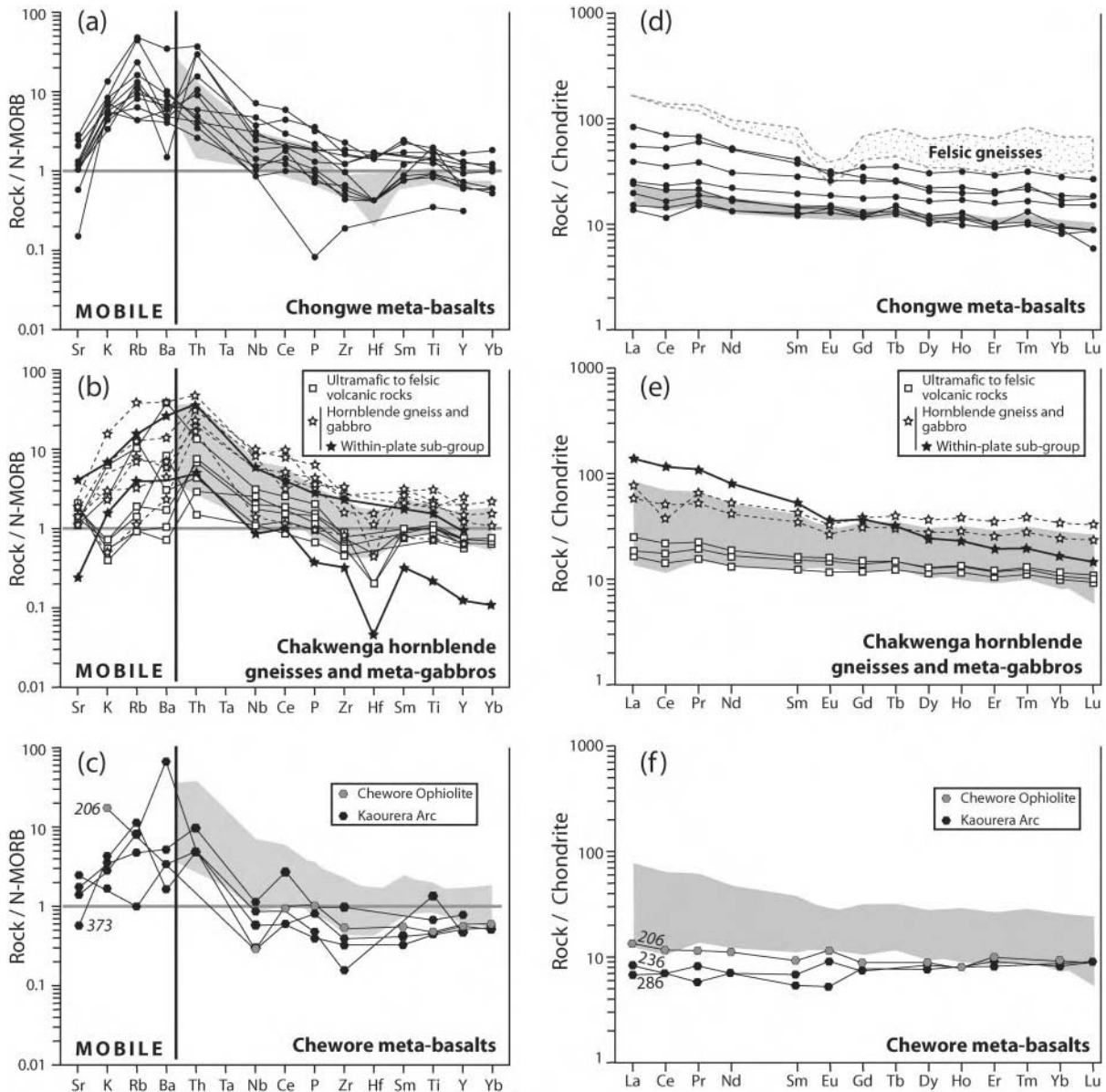


Fig. 7. (a–c) N-MORB-normalized (after Pearce, 1983) trace-element patterns for metabasalts from the Chakwenga, Chongwe and Chewore complexes (data are given in Table 1). The shaded field in (a) represents the range of data from the Chakwenga Complex, those in (b) and (c) represent data range from the Chongwe Complex. (d–f) Chondrite-normalized (after Nakamura, 1974) REE patterns for metabasalt lithologies in the Chakwenga, Chongwe and Chewore complexes (data are given in Table 1). The shaded field in (d) represents the range of data from the Chakwenga Complex, those in (e) and (f) represent data range from the Chongwe Complex.

ZIRCON U–Pb SHRIMP GEOCHRONOLOGY

Data for six Chongwe and one Chakwenga Complex sample are presented.

The Chongwe Complex

Sample C6 (*banded mafic gneiss*)

The abundant zircons extracted from this sample range in size from 100 to 300 μm , have length to width ratios from

2:1 to 3:1 and, in general, are euhedral with typical bipyramidal terminations. Cathodoluminescence (CL) imaging reveals that many grains contain oscillatory-zoned cores surrounded by unzoned to sector zoned rims up to 70 μm in thickness (Fig. 9a). U–Pb analyses were made on five core regions and six rims. Proportions of common ^{206}Pb in total ^{206}Pb (f^{206}) range from 0.00 to 0.19% for all analyses, except for the core region of zircon c6-1c, which has an elevated f^{206} of 2.61% (Table 2). U and Th contents for the core analyses were in the range of 286–572 ppm

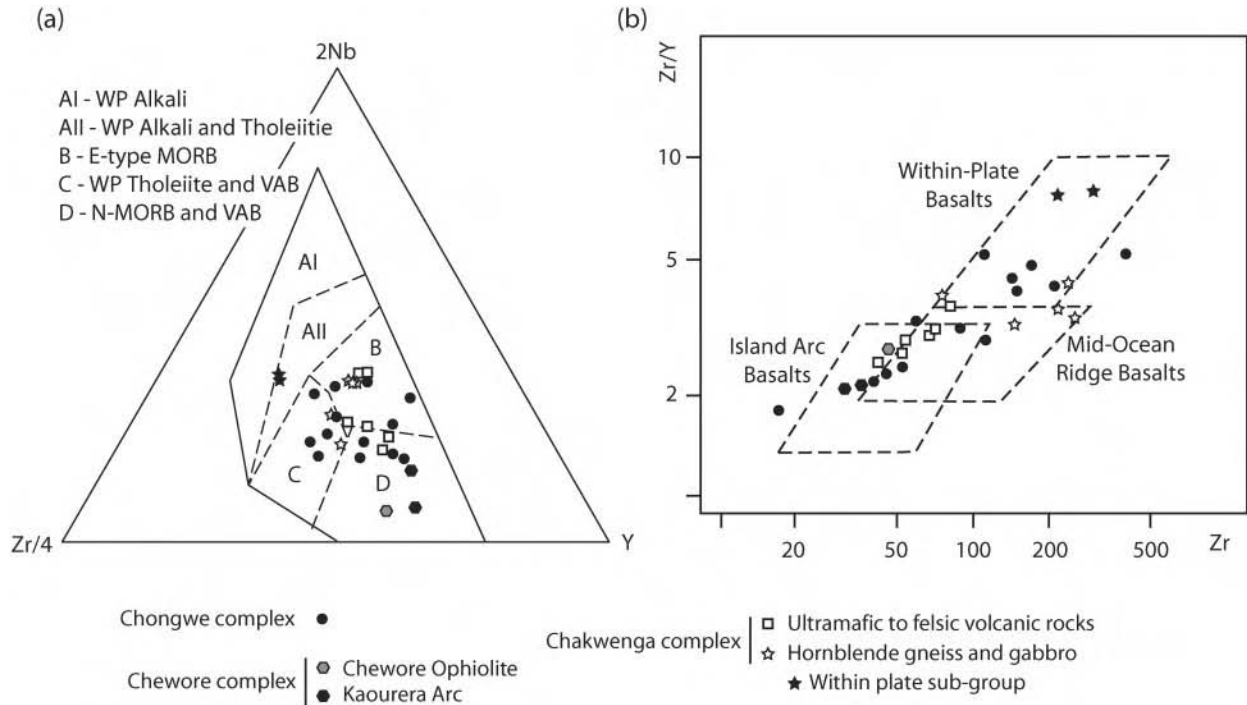


Fig. 8. Basalt tectonic discrimination diagrams after (a) Pearce & Norry (1979) and (b) Meschede (1986). The data scatter widely, suggesting various tectonic settings for the metabasalts. However, isotopic and REE data indicate that the parental magmas to the metabasalts have a common depleted mantle source and have been variably contaminated by older, isotopically homogeneous, incompatible trace element-rich felsic continental crust. In this scenario, the distribution of points in the tectonic discrimination diagram is controlled by the degree of contamination and does not reflect the original tectonomagmatic setting; therefore, without the consideration of isotopic or REE data, these diagrams can be misleading and should be used with caution. WP, within plate; VAB, volcanic arc basalt.

and 149–335 ppm, respectively, leading to Th/U ratios of 0.5–0.6, which are typical for magmatic zircon (Rubatto & Gebauer, 2000). The U contents of the rims were much higher (719–1051 ppm) and Th contents much lower (61–93 ppm) than those of the magmatic cores, leading to Th/U ratios (0.06–0.12) consistent with their growth during a metamorphic event (Rubatto & Gebauer, 2000). Except for core analysis c6-1c, which has high f_{206} and exhibits significant reverse discordance (110%), the remaining core analyses are within 3% of concordia (97–102% concordant) and yield a concordia age of $c. 1050$ Ma. The six remaining core analyses regress to a mean $^{207}\text{Pb}/^{206}\text{Pb}$ age of 1051 ± 12 Ma [mean square weighted deviation (MSWD) = 0.43] (Fig. 10a), which we interpret to be the age of igneous crystallization of the gneiss. The six rim analyses plot on concordia and yield a concordia age of 573 ± 2 Ma (MSWD = 0.106), which we interpret to be the age of amphibolite-facies metamorphism and which is consistent with other Pan-African metamorphic ages in the region (Johnson *et al.*, 2005).

Sample C9a (leucocratic garnet-bearing gneiss–metadacite)

Zircons from this sample are sub-spherical to elongate in shape with the longest axis being between 50 and 150 μm in length. Imaging under CL conditions reveals the

presence of rounded oscillatory-zoned to sector-zoned cores, which are surrounded by CL bright rims up to 50–100 μm wide (Fig. 9b). We have analysed six zircons, including two core–rim pairs (c9-1 and c9-2), one rim (c9-3r) and three single-sector zircons (c9-4, c9-9 and c9-10). The proportion of f_{206} for all analyses is very low, between 0.00 and 0.21% (Table 2). U and Th contents vary in the range of 95–483 ppm and 50–93 ppm, respectively, for the cores and single-sector zircon, resulting in variable Th/U between 0.06 and 0.58. The rims display the lowest U and Th values (24–75 and 3–29 ppm, respectively), and have widely variable Th/U ratios (0.06–1.24; Table 2). The data range from strongly discordant to reversely discordant, with the three rim analyses displaying the highest discordance. The data define a poorly constrained discordia that intercepts the concordia line at 1046 ± 24 Ma and 166 ± 110 Ma (MSWD = 0.5) (Fig. 10b). Given the variable discordance and poor clustering of the data, the upper intercept age can only be taken as a very preliminary estimate of the crystallization age of zircon in the volcanic precursor rock of sample C9.

Sample C10 (K-feldspar augen gneiss)

The majority of zircons extracted from this rock are sub-rounded to elongate, between 100 and 150 μm in length,

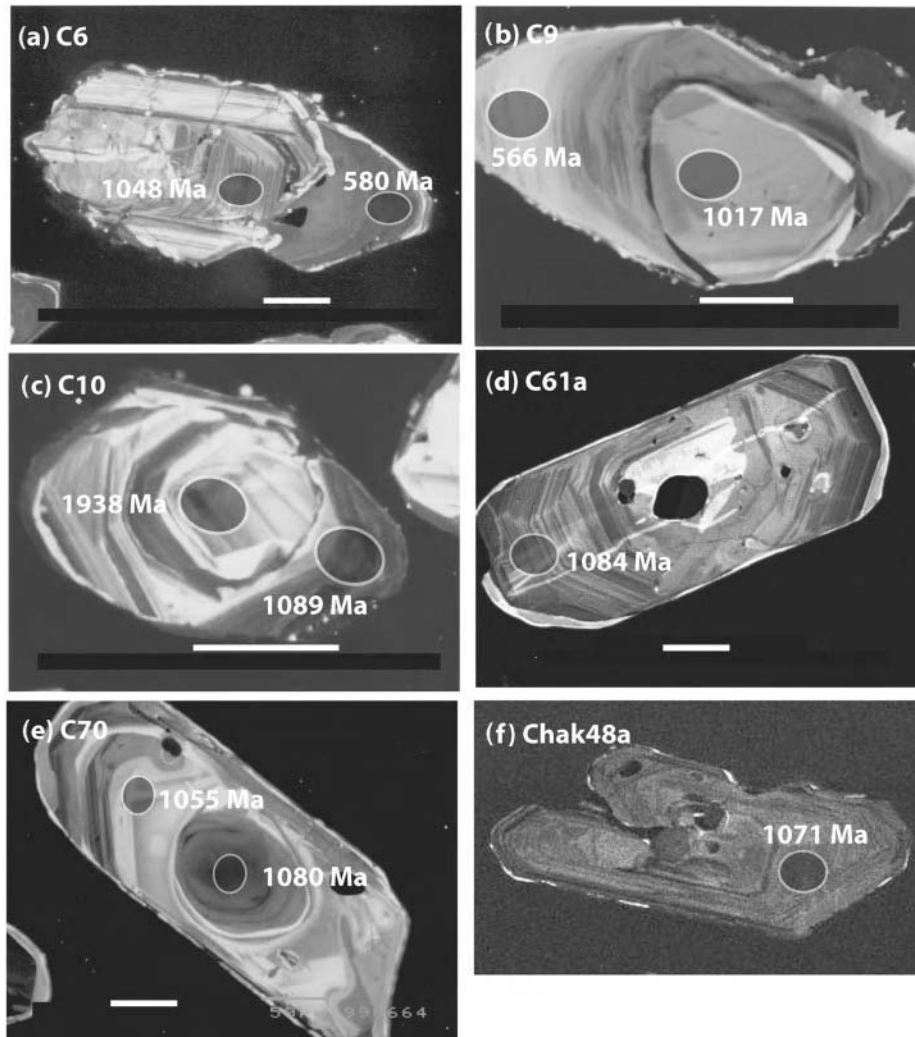


Fig. 9. Cathodoluminescence images of representative zircons from the six dated samples: (a–e) from the Chongwe Complex; (f) from the Chakwenga Complex. Shaded elliptical regions show the area analysed by the SHRIMP. White scale bar in each plate represents 50 μm . The isotopic and age data are given in Table 2 and detailed textural and age analyses are presented in the main text.

with length to width ratios of $\sim 2:1$. Rare grains exhibit bipyramidal terminations typical of an igneous origin. CL imaging reveals that most grains contain cores and rims, both displaying oscillatory zoning (Fig. 9c). We have analysed eight grains, seven rims, two cores and a single grain that does not contain any rim. The proportion of f^{206} is low (between 0.00 and 0.47%) and there is no obvious systematic difference in U and Th content between cores and rims, all analyses having 289–1819 ppm U, 5–517 ppm Th and Th/U ratios between 0.01 and 1.32 (Table 2). The single grain (c10-1), and two cores (c10-5c, c10-6c) have Palaeoproterozoic $^{207}\text{Pb}/^{206}\text{Pb}$ ages of 1917 ± 5 Ma (c10-1, 99% concordant), 1938 ± 8 Ma (c10-6c, 96% concordant) and 1809 ± 6 Ma (c10-5c, 98% concordant) (Fig. 10c) and are interpreted to be inherited grains. It is interesting to note that these three grains have the

highest Th/U ratios of 1.32, 1.07 and 0.83, respectively, whereas the remaining core and rim analyses all have low to very low Th/U ratios of 0.003–0.01 and late Mesoproterozoic ages. Zircons with Th/U ratios < 0.1 are usually considered to be of metamorphic origin (Rubatto & Gebauer, 2000); however, the oscillatory zoning displayed by both cores and rims strongly suggests that they are magmatic. Analysis c10-5r, which has the largest f^{206} value of 0.47%, is reversely discordant (112%) and is not open to easy interpretation. Except for analysis c10-7r, which has a slightly older $^{207}\text{Pb}/^{206}\text{Pb}$ age of 1105 ± 9 Ma, the remaining core and rim analyses form a single age population with a weighted mean $^{207}\text{Pb}/^{206}\text{Pb}$ age of 1092 ± 9 Ma (MSWD = 0.9) and a concordia age of 1094 ± 2 Ma ($n = 5$, MSWD = 0.055) (Fig. 10c). The low MSWDs for both the pooled $^{207}\text{Pb}/^{206}\text{Pb}$ and concordia

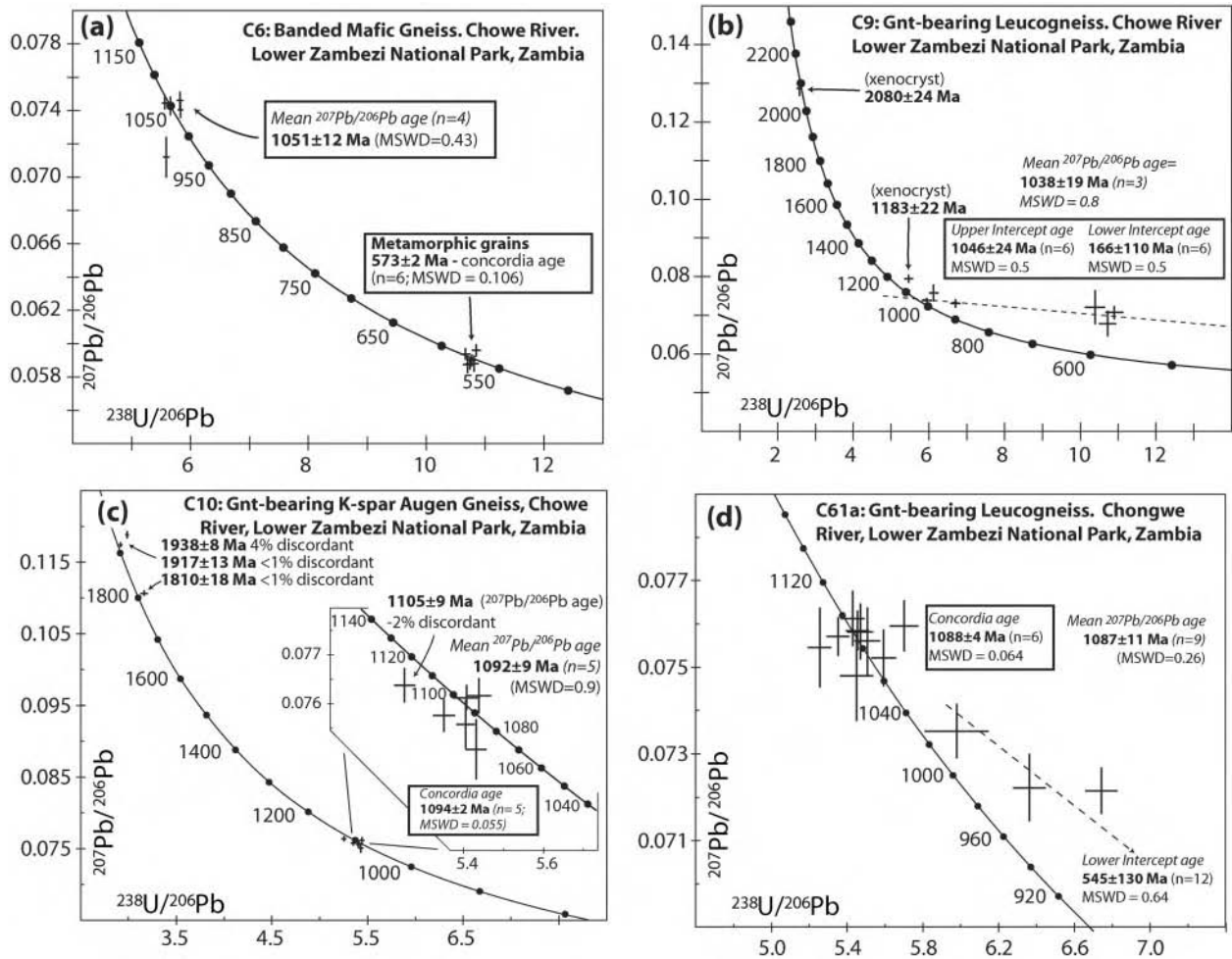


Fig. 10. Tera–Wasserburg U–Pb concordia diagrams for the six samples from the Chongwe and Chakwenga complexes.

age indicate the coherence of the data and lend confidence to the interpretation that the igneous protolith crystallized at *c.* 1094 Ma.

Sample C61a (*leucocratic garnet-bearing gneiss*)

All zircons extracted from this sample are elongate (200–300 μm in length), euhedral grains with typical igneous bipyramidal terminations (Fig. 9d). Most grains contain 10–50 μm sized inclusions typical of zircon from volcanic rocks (Thomas *et al.*, 2003). CL images indicate that all the grains are oscillatory-zoned and only very thin (<10 μm), bright (in CL) rims have been detected around the margins of some grains. U–Pb analyses of these rims are beyond the spatial resolution of the SHRIMP. We have analysed 12 separate grains and all have very low f_{206} values (0.00–0.13) and are relatively uniform in U and Th concentrations (118–307 ppm U and 64–218 ppm Th) with Th/U ratios between 0.43 and 0.90

(Table 2). Apart from three variably discordant analyses (c61a-3, c61a-7 and c61a-11) the remainder define a single, coherent age population with a weighted mean $^{207}\text{Pb}/^{206}\text{Pb}$ age of 1087 ± 11 Ma (MSWD = 0.26) and with the six most concordant grains giving a concordia age of 1088 ± 4 Ma (MSWD = 0.064) (Fig. 10d) which we interpret as the age of crystallization of the igneous rock. The three variably discordant grains define a Pb-loss trend from this crystallization age (*c.* 1088 Ma) toward a lower intercept at *c.* 545 Ma; that is, similar in age to the metamorphic grains in the other samples (Fig. 10d).

Sample C70 (*leucocratic garnet-bearing gneiss*)

Similar to sample C61a, all extracted zircons were clear, euhedral grains, 200–300 μm in length, with typical igneous bipyramidal terminations. All grains show oscillatory zoning under CL conditions and no core–rim relationships were observed (Fig. 9e). We analysed five grains

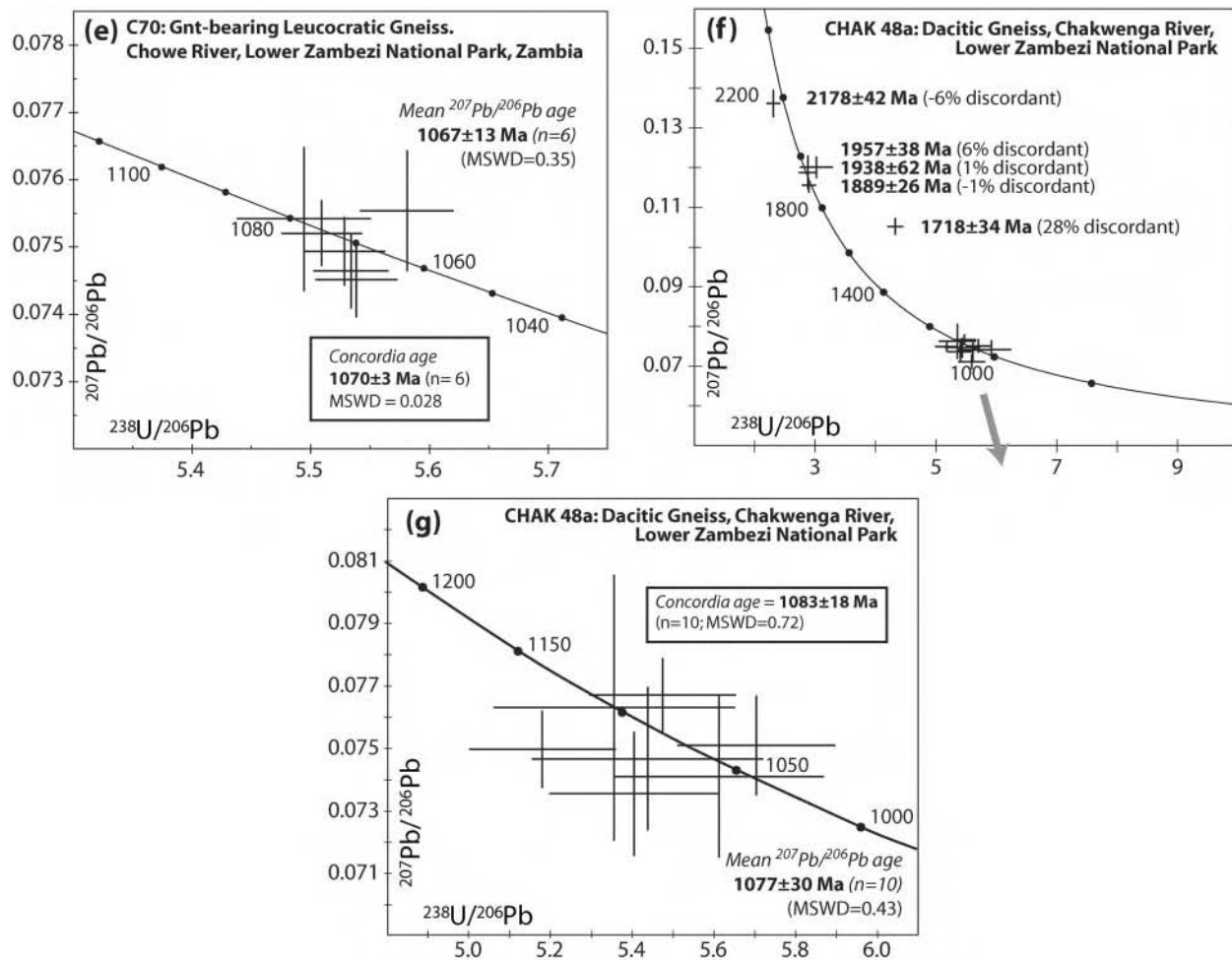


Fig. 10. Continued.

all of which have low f_{206} values (0.00–0.04%) and uniform U and Th concentrations (114–324 ppm U and 97–206 ppm Th) with Th/U ratios of 0.42–0.88 (Table 2). All five grains are part of a single population that gave a mean weighted $^{207}\text{Pb}/^{206}\text{Pb}$ age of 1067 ± 13 Ma (MSWD=0.35) and a concordia age of 1070 ± 3 Ma (MSWD=0.028) (Fig. 10e), which we interpret to be the age of crystallization of the igneous protolith.

Chakwenga Complex

Sample Chak48a (meta-dacitic gneiss)

Zircons extracted from this sample were elongate (75–200 μm in length) with length to width ratios of 3:1 to 4:1 but generally showed rounded and abraded terminations (Fig. 9f) and contain numerous, small (<10 μm) inclusions. Imaging under CL showed that all grains were oscillatory-zoned and no core–rim relationships have been observed. We have analysed 15 grains and most have low f_{206} values between 0.00 and 1.29 and relatively low concentrations of U and Th (68–388 ppm U and

54–334 ppm Th) with Th/U ratios between 0.52–2.20 (Table 2). Ten grains define a single coherent age population with a mean weighted $^{207}\text{Pb}/^{206}\text{Pb}$ age of 1077 ± 30 Ma (MSWD=0.43) and a concordia age of 1083 ± 18 Ma (MSWD=0.72) (Fig. 10f and g) that we interpret to be the age of crystallization of the igneous rock. Five other grains give Palaeoproterozoic ages and we interpret these grains to be inherited. Grain Chak48-4c has a very discordant (78% concordant) $^{207}\text{Pb}/^{206}\text{Pb}$ age of 1718 ± 34 Ma, Chak48-6 has a $^{207}\text{Pb}/^{206}\text{Pb}$ age of 2178 ± 42 Ma (106% concordant), Chak48-7 has a $^{207}\text{Pb}/^{206}\text{Pb}$ age of 1889 ± 26 Ma (101% concordant), Chak48-8 has a $^{207}\text{Pb}/^{206}\text{Pb}$ age of 1957 ± 38 Ma (94% concordant) and Chak48-11 has a $^{207}\text{Pb}/^{206}\text{Pb}$ age of 1938 ± 62 Ma (99% concordant) (Fig. 10f and g).

WHOLE-ROCK AND ZIRCON ISOTOPES

Twenty-one samples of variable SiO_2 composition and age from the Chakwenga, Chongwe and Chewore complexes

were selected for whole-rock Sm–Nd and Rb–Sr isotopic analysis; additionally, inherited zircons from samples of Chongwe and Chakwenga leucocratic gneiss were analysed for their Lu–Hf isotope composition. Seven of the samples have well-constrained crystallization ages, but the precise ages of the remaining 14, mainly meta-basaltic samples, are unknown. Considering the relatively restricted time period (*c.* 1090–1040 Ma) for magmatism within the Chewore–Rufunsa Terrane documented here and for the SIB in general (Johnson *et al.*, 2006), it is appropriate to provide only maximum and minimum initial isotopic ratios for these samples calculated using the oldest (*c.* 1090 Ma) and youngest (*c.* 1040 Ma) determined magmatic ages. Five inherited zircon grains, all of Palaeoproterozoic age, were selected for *in situ* Lu–Hf analysis, to gain information on the isotopic composition of the basement into which these magmas were intruded and to constrain contamination–assimilation pathways.

The Chakwenga Complex

The measured whole-rock $^{147}\text{Sm}/^{144}\text{Nd}$ ratios for all samples lie between 0.119 and 0.180 (Table 3). The dated felsic sample Chak48a (1083 Ma) has an initial $^{143}\text{Nd}/^{144}\text{Nd}$ ratio of 0.51072, $\epsilon_{\text{Nd}(t)}$ values of -10.14 and a TDM age of 2.34. The remaining three meta-felsic lithologies, which encompass the mafic to felsic volcanic rocks, hornblende gneiss and gabbro, have initial $^{143}\text{Nd}/^{144}\text{Nd}_{(1090-1040)}$ values between 0.51077 and 0.511215 with $\epsilon_{\text{Nd}(1090-1040)}$ values ranging between $-0.62_{(1090)}$ to $-9.12_{(1090)}$ and $-0.82_{(1040)}$ to $-9.63_{(1040)}$ (Table 3; Fig. 11a). The same samples give T_{DM} model ages between 1.73 and 2.50 Ga. The initial whole-rock $^{87}\text{Sr}/^{86}\text{Sr}$ ratios for all samples lie between 0.691 and 0.726. The lower values indicate that the Rb/Sr ratios may have been altered during amphibolite-facies metamorphism; therefore, little emphasis can be placed on them. Four inherited zircon grains from sample Chak48a (6, 7, 8, 11) with $^{207}\text{Pb}/^{206}\text{Pb}$ ages of *c.* 1889–2178 have initial $^{176}\text{Hf}/^{177}\text{Hf}(t)$ ratios between 0.28148 and 0.28169 with $\epsilon_{\text{Hf}(i)}$ values ranging between $+2.9$ and -3.7 (Table 4).

The Chongwe Complex

Two meta-basaltic samples (C6 and C64), two meta-andesitic samples (C7 and C61b) and three felsic lithologies (C9a, C61a and C62b) were analysed. The measured whole-rock $^{147}\text{Sm}/^{144}\text{Nd}$ ratios for all samples have a similar range to those from the Chakwenga Complex, between 0.115 and 0.179 (Table 3). The dated meta-mafic lithology, sample C6 (1051 Ma), has an initial $^{143}\text{Nd}/^{144}\text{Nd}$ ratio of 0.511188, an $\epsilon_{\text{Nd}(t)}$ value of -1.82 and a T_{DM} model age of 1.90 Ga. The two felsic samples, C9a and C61a, with ages of 1040 Ma and 1088 Ma, have initial $^{143}\text{Nd}/^{144}\text{Nd}$ ratios of 0.510886 and 0.511064, $\epsilon_{\text{Nd}(t)}$ values of -8.02 and -3.31 , and T_{DM} model ages of 2.27 Ga and 1.92 Ga, respectively. The remaining undated mafic to

felsic samples have initial $^{143}\text{Nd}/^{144}\text{Nd}_{(1090-1040)}$ values between 0.510874 and 0.51307, $\epsilon_{\text{Nd}(1090-1040)}$ values ranging from $1.44_{(1090)}$ and $-7.03_{(1090)}$ to $1.28_{(1040)}$ and $-7.50_{(1040)}$, and give T_{DM} model ages between 1.74 and 2.35 Ga. The whole-rock $^{87}\text{Sr}/^{86}\text{Sr}$ ratios for all samples lie between 0.711 and 0.762 and the initial $^{87}\text{Sr}/^{86}\text{Sr}$ ratios for samples C6, C9a and C61a are 0.714, 0.716 and 0.718, respectively. The remaining samples have $^{87}\text{Sr}/^{86}\text{Sr}_{(1090-1040)}$ ratios between 0.697–0.712₍₁₀₉₀₎ and 0.698–0.713₍₁₀₄₀₎. One grain from sample C9a (C9a-4c) with an age of *c.* 2080 Ma has an initial $^{176}\text{Hf}/^{177}\text{Hf}(t)$ ratio of 0.28146 and an $\epsilon_{\text{Hf}(i)}$ value of -0.9 (Table 4).

The Chewore Complex

Four meta-basaltic samples (165, 236, 286, 373) and one felsic sample (220a) from the Kaourera Arc, and one meta-basaltic sample (206) from the Chewore Ophiolite were analysed for their whole-rock isotopic compositions. The geochemical data for these samples were previously presented by Johnson & Oliver (2000, 2004) and are also shown in Fig. 7c and f. The four Kaourera Arc metabasalts have whole-rock $^{147}\text{Sm}/^{144}\text{Nd}$ ratios between 0.1582 and 0.2240 with initial $^{143}\text{Nd}/^{144}\text{Nd}_{(1090-1040)}$ ratios of 0.51108–0.51571 and $\epsilon_{\text{Nd}(1090-1040)}$ values ranging between $+5.2$ to -3.22 and $+5.38$ to -1.36 (Table 3; Fig. 11a and b). Three of these samples have measured $^{143}\text{Nd}/^{144}\text{Nd}$ values close to, or higher than present-day value of CHUR (0.512638; Goldstein *et al.*, 1984) and so give erroneous model ages (Table 3), but sample 165 with lower values provides a T_{DM} age of 2.15 Ga. The felsic sample (220a) dated at *c.* 1082 Ma (Johnson & Oliver, 2004) has an initial $^{143}\text{Nd}/^{144}\text{Nd}$ ratio of 0.510553, an $\epsilon_{\text{Nd}(t)}$ value of -13.47 (Table 3) and a measured $^{143}\text{Nd}/^{144}\text{Nd}$ ratio greater than present-day CHUR, precluding the calculation of a reliable model age. The metabasalt from the Chewore Ophiolite, which has an age of *c.* 1393 (Oliver *et al.*, 1998), has an initial $^{143}\text{Nd}/^{144}\text{Nd}$ ratio of 0.510880, an $\epsilon_{\text{Nd}(t)}$ value of $+1.01$ (Table 1) and a T_{DM} age of 2.02 Ga. Initial Sr values for all samples range between 0.693 and 0.718.

DISCUSSION

Tectonomagmatic origin of the volcano-plutonic suites

Major-element, trace-element and REE geochemistry

Lithologies from the Chongwe and Chakwenga complexes form a supracrustal to mid-crustal volcano-plutonic suite ranging from basalt to rhyodacite or rhyolite (Fig. 6a–h). The samples dated in this study indicate that magmatism occurred in a *c.* 50 Myr time frame from 1090 to 1040 Ma, the same time interval in which volcano-plutonic complexes formed in the other Southern Irumide Belt (SIB) terranes (Table 5; Johnson *et al.*, 2006).

Table 3: Whole-rock Sm–Nd and Rb–Sr isotopic data for meta-igneous lithologies in the Chewore–Rufunsa Terrane

Sample	SiO ₂ (wt%)	Age (Ma)	Measured			Initial			T _{Dm} (Ga)	Measured			Initial							
			Nd (ppm)	Sm (ppm)	¹⁴⁷ Sm/ ¹⁴⁴ Nd	¹⁴³ Nd/ ¹⁴⁴ Nd	¹⁴³ Nd/ ¹⁴⁴ Nd(T)	¹⁴³ Nd/ ¹⁴⁴ Nd(1090)		¹⁴³ Nd/ ¹⁴⁴ Nd(1040)	ε _{Nd(T)}	ε _{Nd(1090)}	ε _{Nd(1040)}	Sr (ppm)	Rb (ppm)	⁸⁷ Rb/ ⁸⁶ Sr	⁸⁷ Sr/ ⁸⁶ Sr	⁸⁷ Sr/ ⁸⁶ Sr(T)	⁸⁷ Sr/ ⁸⁷ Sr(1090)	⁸⁷ Sr/ ⁸⁷ Sr(1040)
Chongwe Complex																				
C6	52.94	1051	32	8	0.15180	0.51224	0.51119	—	—	—1.82	—	—	1.90	336	100	0.298	0.727	0.714	—	—
C7	55.35	—	26	5	0.11355	0.51179	—	0.51098	0.51102	—	−4.96	−5.49	1.86	66	104	1.582	0.752	—	0.680	0.683
C9a	80.35	1040	13	3	0.13419	0.51180	0.51089	—	—	−8.02	—	—	2.27	108	22	0.199	0.725	0.716	—	—
C61A	72.86	1088	67	15	0.13721	0.51204	0.51106	—	—	−3.31	—	—	1.92	166	40	0.243	0.729	0.718	—	—
C61B	53.16	—	48	14	0.17044	0.51252	—	0.51131	0.51136	—	1.44	1.28	1.74	65	51	0.783	0.732	—	0.697	0.698
C62A	49.49	—	14	4	0.17939	0.51245	—	0.51117	0.51123	—	−1.19	−1.29	2.35	70	13	0.182	0.716	—	0.708	0.708
C62B	68.72	—	31	6	0.12064	0.51174	—	0.51087	0.51091	—	−7.03	−7.50	2.07	308	101	0.328	0.727	—	0.712	0.713
C64	45.87	—	11	3	0.16549	0.51227	—	0.51109	0.51114	—	−2.81	−3.00	2.26	111	23	0.206	0.716	—	0.706	0.707
Chakwenga Complex																				
<i>North of UTM 8290</i>																				
31	48.32	—	8	2	0.18040	0.51245	—	0.51116	0.51121	—	−1.48	−1.58	2.44	166	3	0.017	0.711	—	0.710	0.710
35	44.75	—	10	3	0.17799	0.51239	—	0.51112	0.51117	—	−2.29	−2.41	2.50	219	4	0.017	0.711	—	0.710	0.710
52	65.41	—	36	7	0.11438	0.51158	—	0.51077	0.51080	—	−9.12	−9.63	2.16	98	154	1.572	0.762	—	0.691	0.694
54	51.89	—	12	3	0.16636	0.51231	—	0.51112	0.51117	—	−2.21	−2.40	2.20	245	2	0.008	0.712	—	0.712	0.712
<i>South of UTM 8290</i>																				
38	75.00	—	98	19	0.11975	0.51195	—	0.51109	0.51113	—	−2.63	−3.12	1.73	217	67	0.311	0.719	—	0.705	0.701
46	46.93	—	25	7	0.16442	0.51238	—	0.51120	0.51125	—	−0.62	−0.82	1.95	170	7	0.039	0.712	—	0.711	0.711
48A	67.96	1083	33	7	0.12394	0.51160	0.51072	—	—	−10.14	—	—	2.34	242	27	0.112	0.731	0.726	—	—
62	67.24	—	59	12	0.11966	0.51183	—	0.51098	0.51102	—	−5.01	−5.48	1.90	268	106	0.395	0.728	—	0.710	0.711
Chewore Complex																				
165	49.70	—	13	3	0.15819	0.51221	—	0.51108	0.51113	—	−2.97	−3.22	2.15	216	10	0.046	0.713	—	0.711	0.711
206	47.48	1393	9	3	0.17542	0.51249	0.51088	—	—	1.01	—	—	2.02	223	123	0.552	0.725	0.693	—	—
220a	66.14	1082	16	9	0.33018	0.51290	0.51055	—	—	−13.47	—	—	−0.31*	61	6	0.098	0.720	0.716	—	—
236	48.51	—	4	1	0.20764	0.51258	—	0.51110	0.51117	—	−2.57	−2.50	5.53*	172	17	0.099	0.710	—	0.705	0.706
286	49.73	—	5	2	0.20184	0.51260	—	0.51116	0.51123	—	−1.40	−1.36	3.82*	296	2	0.007	0.712	—	0.711	0.711
373	42.49	—	5	2	0.22400	0.51310	—	0.51150	0.51157	—	5.20	5.38	−1.12*	67	23	0.343	0.733	—	0.717	0.718

*Samples with measured ¹⁴³Nd/¹⁴⁴Nd ratios greater than, or close to the Chondritic Uniform Reservoir (present-day value ~0.512638; Goldstein *et al.*, 1984) commonly yield inaccurate or erroneous model ages.

Reliable neodymium isotopic model ages could only be calculated for the precisely SHRIMP-dated samples. For the undated samples, only maximum and minimum estimates could be calculated, based on the age range obtained from the Chewore–Rufunsa Complex (this study) and Southern Irumide Belt (Johnson *et al.*, 2006).

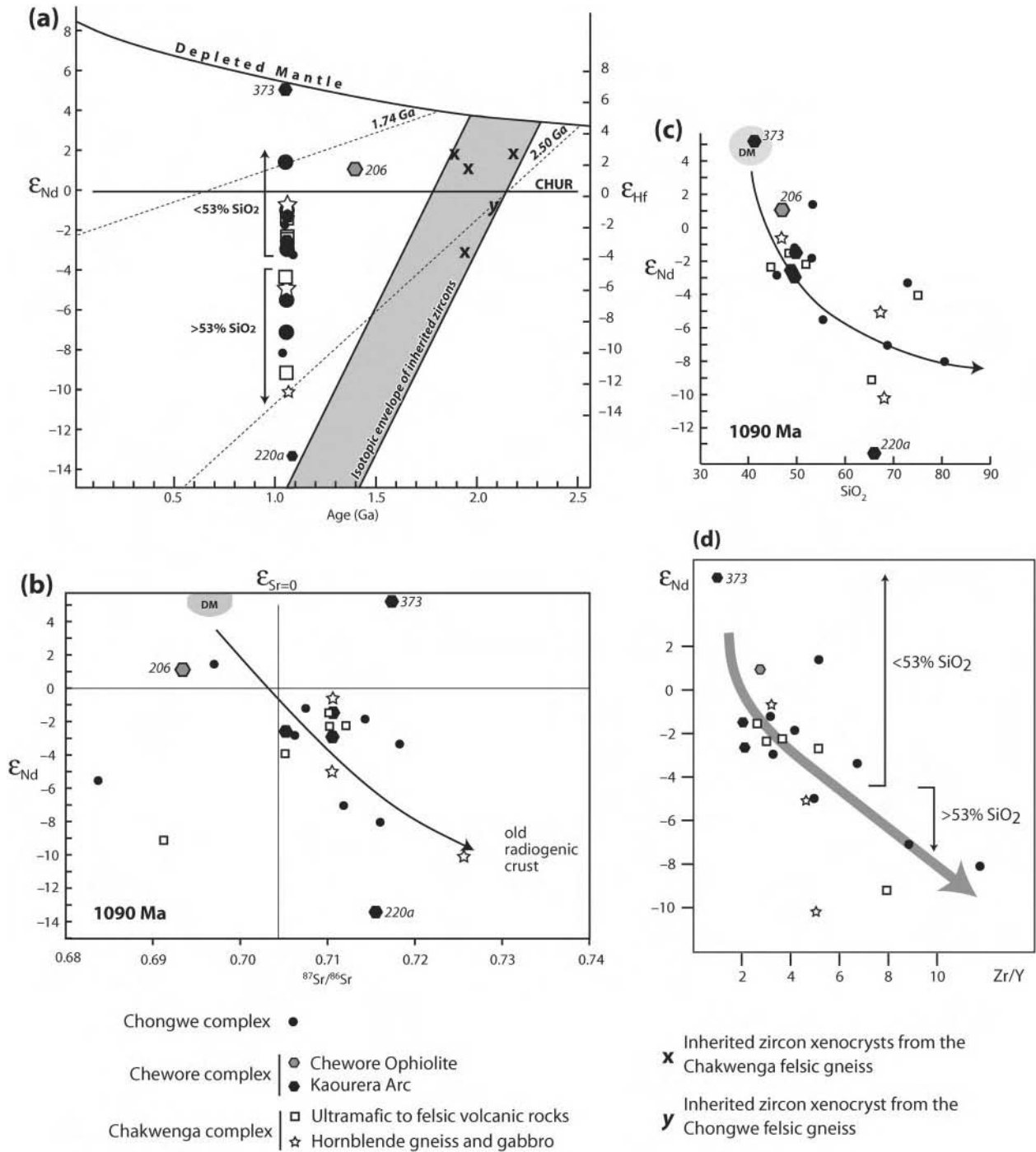


Fig. 11. (a) Nd and Hf isotopic evolution diagram for the whole-rock samples (Sm–Nd) and inherited zircon cores (Lu–Hf). Whole-rock Sm–Nd data for the Chongwe, Chakwenga and Chewore complexes are given in Table 3 and *in situ* Lu–Hf data for inherited zircon cores from the Chongwe and Chakwenga complexes in Table 4. T_{DM} evolution lines were calculated from the Sm–Nd isotopic decay scheme as calculated in Table 3. Small symbols (dots, squares, stars and hexagons) are for the precisely dated samples; larger symbols are for the undated samples and cover the 1090–1040 Ma age range. (b) Nd–Sr evolution diagram for *c.* 1090 Ma. Arrow indicates a schematic trend of mixing between juvenile mafic magmas derived from depleted mantle (DM) and radiogenic Palaeoproterozoic crust. (c) Nd isotopic composition vs SiO_2 content (wt %) of whole-rocks illustrating that with increasing SiO_2 content the samples have increasingly negative $\epsilon_{Nd(t)}$ values. (d) Nd isotopic composition vs Zr/Y illustrating that with increasing Zr/Y ratios the samples have increasingly negative $\epsilon_{Nd(t)}$ values. This relationship would not be expected if the range of samples were produced by simple fractional crystallization processes.

Table 4: In situ Lu–Hf isotopes of inherited zircon from the Chongwe and Chakwenga complexes

Spot	Age (Ma)	$^{176}\text{Hf}/^{177}\text{Hf}$	Error (2 σ)	$^{176}\text{Hf}/^{177}\text{Hf}(i)$	Error (2 σ)	$\epsilon_{\text{Hf}(t)}$
C9-4c	2080	0.28149306	2.546E - 05	0.28146481	2.545E - 05	-0.9
CHAK48a-7	1889	0.28172841	2.333E - 05	0.28169650	2.329E - 05	2.8
CHAK48a-11	1938	0.28154200	2.213E - 05	0.28148110	2.252E - 05	-3.7
CHAK48a-8	1957	0.28164066	5.137E - 05	0.28162350	5.139E - 05	1.8
CHAK48a-6	2178	0.28154481	2.871E - 05	0.28150594	2.880E - 05	2.9

Table 5: Summary of the reliable SHRIMP U–Pb zircon crystallization ages for meta-igneous lithologies in the Southern Irumide Belt

Sample	Location	Lithology	Age (Ma)	Reference
<i>Chewore–Rufunsa Terrane</i>				
C6	Chongwe	Layered mafic gneiss	1051 ± 12	This study
C9a	Chongwe	Felsic gneiss	1038 ± 19	
C10	Chongwe	K-feldspar augen gneiss	1094 ± 2	
C61a	Chongwe	Felsic gneiss	1088 ± 4	
C70	Chongwe	Felsic gneiss	1070 ± 3	
CHAK48a	Chakwenga	Felsic gneiss	1083 ± 18	
SJ220	Chewore	Metadacite	1082 ± 7	Johnson & Oliver (2004)
SJ106.1	Chewore	Plagiogranite dykes	1393 ± 22	Oliver <i>et al.</i> (1998)
Kadunguri	Chewore	Whiteschist	1066 ± 22	S. P. Johnson (unpublished data)
Whiteschists				
ADC	Chewore	Quartzo-feldspathic orthogneiss	1071 ± 8	Goscombe <i>et al.</i> (2000)
AF	Chewore		1083 ± 8	
<i>Nyimba Terrane</i>				
NY82		Pelitic migmatite	2000–1800	Johnson <i>et al.</i> (2006)
<i>Petauke–Sinda Terrane</i>				
PS65		Porphyritic granite	1043 ± 14	Johnson <i>et al.</i> (2006)
SZ16		Pelitic migmatite	1984 ± 21	
SZ23		Quartzo-feldspathic orthogneiss	1008 ± 17	
SZ25c		Mylonitized porphyritic granite	1023 ± 12	
SZ26		Quartzo-feldspathic orthogneiss	1961 ± 31	
<i>Chipata Terrane</i>				
CHP2a		Augen gneiss	1046 ± 4	Johnson <i>et al.</i> (2006)
CHP2c		Syenite	1050 ± 7	
CHP4a		Felsic granulite	1076 ± 6	
CHP4b		Mafic xenolith	1977 ± 11	
CHP5		Felsic granulite	1047 ± 20	
CHP6a		Hornblende-bearing granite	1038 ± 6	
CHP8		Porphyritic granite	1061 ± 13	
CHP10		Porphyritic granite	1076 ± 14	
CHP11a		Migmatite	1950 ± 67	
CHP12		Porphyritic granite	1038 ± 9	
CHP13		Porphyritic granite	1058 ± 34	

Mafic to felsic lithologies in the Chewore Complex (Fig. 1) were interpreted to have formed in an island-arc setting by Johnson & Oliver (2004) and their major, trace and REE compositions were related to simple, closed-system fractional crystallization. The major- and trace-element data for the Chongwe–Chakwenga lithologies are similar to those of the Chewore Complex, but in contrast they generally have higher abundances of the immobile trace elements and exhibit greater variability at any given SiO_2 composition (Figs 6b–h and 7a–c). The Chongwe–Chakwenga and Chewore metabasalts have similar, parallel REE profiles, but the Chongwe–Chakwenga metabasalts have higher REE concentrations that become progressively LREE-enriched with increasing REE content (Fig. 7d–f). The hornblende gneisses and metabasalts from the southern part of the Chakwenga Complex have enriched REE concentrations compared with the finer-grained volcanic lithologies in the northern part, but they too have REE profiles that are parallel to the metabasalt trends and overlap with the Chongwe Complex rocks. Overall the similar N-MORB-normalized and chondrite-normalized REE patterns for all the plutonic and volcanic rocks from both areas suggest that they formed in the same tectonomagmatic environment. The Chewore metabasalts have the lowest REE and trace-element concentrations and are the least evolved of all the analysed basaltic lithologies. Their prominent negative Nb anomaly (Fig. 7c), when normalized to N-MORB (Johnson & Oliver, 2004), suggests the parental melts formed in a supra-subduction-zone environment. The Chongwe–Chakwenga metabasalts appear to represent similar supra-subduction-zone magmas, which were variably contaminated by a highly evolved source, probably felsic crust of similar composition to the Chongwe felsic gneisses (Fig. 7d). This would explain the lack of distinct negative Nb anomalies in the Chongwe–Chakwenga metabasalts (Fig. 7a and b). Thus their whole-rock major- and trace-element, and REE chemistry can be explained by simple two-component mixing or assimilation between a primary mafic supra-subduction-zone magma, similar in composition to the Chewore metabasalts, and a highly evolved felsic crustal end-member (i.e. local continental crust). Two samples from the northernmost part of the Chakwenga Complex (samples 37a and 37b) have distinctly different N-MORB-normalized and chondrite-normalized REE profiles (Fig. 7b and e). Although these samples have similar immobile trace-element concentrations to the other Chongwe and Chakwenga metabasalts, their element ratios (Fig. 8) and REE patterns suggest that they formed in a within-plate tectonic setting. As the crystallization age of these samples is not known it is difficult to speculate on their tectonic significance and whether or not they are an integral part of the Chakwenga volcano-

magmatic complex or are significantly younger and related to crustal extension processes identified elsewhere in the SIB (Johnson *et al.*, 2006, 2007).

Whole-rock Sm–Nd and Rb–Sr isotopes

Taken together, the samples show a wide range of initial $^{143}\text{Nd}/^{144}\text{Nd}$ ratios and $\epsilon_{\text{Nd}(t)}$ values that are not easily related to their age, location, trace-element or REE composition (Table 3; Fig. 11a). In general, the meta-basaltic lithologies have less evolved (i.e. juvenile) $\epsilon_{\text{Nd}(t)}$ isotopic signatures, ranging from +5 to –4, whereas those with >53 wt % SiO_2 have the most enriched signatures with $\epsilon_{\text{Nd}(t)}$ values between –5 and –14 (Table 3; Fig. 11a and c). In an ϵ_{Nd} vs $^{87}\text{Sr}/^{86}\text{Sr}_{(i)}$ diagram (Fig. 11b) these samples form a broad linear trend ranging from relatively juvenile to significantly radiogenic compositions; however, the spread in $^{87}\text{Sr}/^{86}\text{Sr}_{(i)}$ data suggests that there may have been some disturbance of the Rb–Sr isotopic system during subsequent high-grade Neoproterozoic metamorphism. The correlations between ϵ_{Nd} and SiO_2 content or Zr/Y ratio (Fig. 11c and d) cannot be explained by simple fractional crystallization processes, as the whole-rock isotopic signature should remain constant during closed-system fractionation processes. In light of the major-, trace-element and REE data, these relationships can be explained by variable degrees of assimilation–contamination of a juvenile mantle-derived mafic magma with an SiO_2 - and incompatible element-rich, radiogenic crustal basement. The age and isotopic character of this basement is constrained by the U–Pb age and Lu–Hf composition of inherited zircons extracted from the felsic lithologies. Figure 12 shows that 15 (95–105% concordant) inherited zircon have Palaeoproterozoic ages that range from *c.* 2.2 to 1.7 Ga, a single grain has a Palaeoproterozoic age of *c.* 2.4 Ga, and another grain has an Archaean age of *c.* 2.9 Ga. This age range can be compared with the Nd isotopic model ages for all of the mafic and felsic volcano-plutonic rocks, which range between 2.50 and 1.74 Ga (Fig. 11a), suggesting that the Palaeoproterozoic basement itself formed by juvenile processes without the significant involvement of older crust. This is confirmed by the admittedly small number of *in situ* Lu–Hf analyses of the inherited zircon grains. Five zircon grains, ranging in age between *c.* 2.2 and 1.85 Ga gave $\epsilon_{\text{Hf}(i)}$ values between +2.9 and –3.7 (Table 4; Fig. 11a) and if these inherited zircons are representative of the age and isotopic composition of the basement, then by late Mesoproterozoic times, this basement would have evolved to an isotopic composition that can adequately account for a two-component mixing–contamination trend between juvenile mantle-like supra-subduction-zone basalts and a relatively isotopically homogeneous Palaeoproterozoic basement (Fig. 11a).

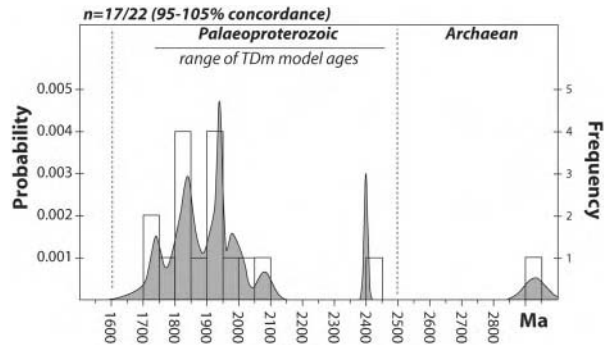


Fig. 12. Histogram and probability-density distribution (pdd) diagram for 22 inherited or xenocrystic zircon from the Chewore–Rufunsa Terrane. Data are from this study, Goscombe *et al.* (2000) and Johnson & Oliver (2004).

Implications for basalt tectonic discrimination diagrams

Over recent decades the use of basalt discrimination diagrams in tectonic studies has increased markedly, especially in the interpretation of mafic meta-igneous rocks from medium- to high-grade metamorphic terranes. In such settings, the application of these discrimination diagrams is above and beyond their intended use; however, in general, diagrams involving the relatively immobile elements Zr, Nb, Y, Hf, Th, Ta, Yb and La (e.g. Pearce & Cann, 1973; Pearce & Norry, 1979; Wood, 1980; Meschede, 1986) have been found to be useful. In this study the ratios of key trace elements such as Zr, Nb and Y (Fig. 6i and j) appear to have been altered by contamination of the parental basalts by continental crust, thus altering the position and ultimately, tectonic field in which they plot (Fig. 8). The situation is more complex if these ratios have also been modified by subsequent metamorphic events. We have found that the chondrite-normalized REE diagrams and Nd isotopic compositions are the most powerful tools in determining the relationship between the volcano-plutonic rocks and ultimately in defining their tectonic setting. We urge caution in the isolated use of tectonic discrimination diagrams and suggest that particular attention is paid to defining magmatic suites based on a number of geochemical and isotopic characteristics.

Regional tectonic setting

The major, trace and REE geochemistry and isotopic composition of the supracrustal to mid-crustal volcano-plutonic rocks that form the Chewore–Runfunsa Terrane indicate formation in a supra-subduction-zone setting in which there was significant contamination by Palaeoproterozoic continental crust, implying a continental-margin-arc setting. *In situ* U–Pb and Lu–Hf analyses of inherited zircon grains from this basement confirm its isotopic homogeneity, having formed via juvenile magmatic processes predominantly between *c.* 2.2 and 1.8 Ga. U–Pb dating places constraints on the initiation and duration of continental-

arc magmatism to between *c.* 1090 and 1040 Ma, but the presence of a *c.* 1393 Ma marginal basin ophiolite in the Chewore Complex (Oliver *et al.*, 1998; Johnson & Oliver, 2000) suggests considerable longevity of supra-subduction magmatism in this region. Reconnaissance U–Pb SHRIMP zircon dating of granitoid lithologies from the other SIB terranes (Johnson *et al.*, 2006) suggests that magmatism, potentially arc-related on the basis of field relations and whole-rock chemistry (Mapani *et al.*, 2001, 2004), occurred throughout this belt at this time, culminating in high-temperature (>850°C), low-pressure (<4 kbar), localized granulite-facies metamorphism. The nature and timing of magmatism and style of tectonometamorphism in the adjoining IB is significantly different from that of the SIB. In the IB, minor granitoid magmatism began at *c.* 1040 Ma and peaked with the intrusion of voluminous granitoids at *c.* 1020 Ma (De Waele, 2005; De Waele *et al.*, 2006b). Although metamorphism proceeded mainly in the andalusite field, peak conditions of ~850°C at ~8 kbar (Mapani & Moore, 1995; De Waele *et al.*, 2005) were obtained in the southern part of the IB, the peak of which has been dated at *c.* 1020 Ma (DeWaele, 2005). This event was accompanied by contractional deformation and substantial crustal thickening (Daly, 1986) and was coincident with the peak of granitoid magmatism. The major- and trace-element and REE chemistry of all the *c.* 1040–1020 Ma granitoids are identical and were produced by the *in situ* melting–recycling of tectonically thickened crust (De Waele *et al.*, 2006a). The distinct tectonomagmatic episodes, apparent cessation of magmatism in the SIB, and the initiation of magmatism and contractional deformation in the IB all contribute to the interpretation that the SIB developed separately from the IB until juxtaposition at *c.* 1040 Ma (Johnson *et al.*, 2006). We suggest that the SIB developed by the subduction of oceanic crust under the margin of an unnamed continental mass. The subsequent closure of this ocean at *c.* 1040 Ma resulted in the juxtaposition–collision of this unnamed continent with the margin of the Congo Craton (specifically the Bangweulu Block), leading to the cessation of arc-magmatism in the SIB, crustal thickening and compressional tectonics along the margin of the Congo Craton and crustal melting to form the voluminous IB batholiths (De Waele *et al.*, 2006a,b; Johnson *et al.*, 2006). The early low-pressure, high-temperature tectonometamorphic development of the IB requires additional heat input into the base of the IB crust before the onset of crustal thickening. Although we lack any empirical data, this observation alone may suggest that ocean closure occurred via two subduction zones, an older one dipping under the SIB (*c.* 1090–1040 Ma) and a younger, hotter slab dipping under the IB (*c.* 1040–1020 Ma). Detailed geochemical and isotopic investigations of the early IB granitoids (*c.* 1040–1020 Ma) would be needed to resolve this issue.

ACKNOWLEDGEMENTS

This paper is dedicated to our recently deceased friend and colleague Crispin Katongo, who will be sorely missed. Sincere thanks go to Willy Nundwe, without whose excellent driving skills, hammering ability, and company none of this would be possible. Thanks also go to the numerous game scouts who accompanied us during the fieldwork. We sincerely thank Toby Rivers, Grahame Oliver and Robin Offler for their constructive reviews and for greatly improving the manuscript. S.P.J. acknowledges research funding from the Tectonics Special Research Center (TSRC), an Australian Research Council IREX fellowship and a Japanese Kaken-Hi grant. This is TSRC m/s number 405 and a contribution to IGCP 418/440.

REFERENCES

- Barr, M. C. W. (1998). *The geology of the Chongwe River area; explanation of degree sheet 1529, SW quarter*. Lusaka: Geological Survey Department of Zambia, 45 pp.
- Brekke, H., Furnes, H., Nordaas, J. & Hertogen, J. (1988). Lower Palaeozoic convergent plate margin volcanism on Bomlo, SW Norway, and its bearing on the tectonic environments of the Norwegian Caledonides. *Journal of the Geological Society, London* **141**, 1015–1032.
- Brouxel, M. & Lapierre, H. (1988). Geochemical study of an early Paleozoic island-arc back-arc basin system. Part I: the Trinity ophiolite (northern California). *Geological Society of America Bulletin* **100**, 1111–1119.
- Cox, R. A., Rivers, T., Mapani, B., Tembo, D. & De Waele, B. (2002). New U–Pb data for the Irumide belt: LAM-ICP-MS results for Luangwa Terrane. In: *11th IAGOD Quadrennial Symposium and Geocongress, Technical Meeting IGCP 440: Assembly and Breakup of Rodinia, Windhoek, Namibia*. Windhoek: Geological Survey of Namibia, 10 pp.
- Daly, M. C. (1986). The intracratonic Irumide belt of Zambia and its bearing on collision orogeny during the Proterozoic of Africa. In: Coward, M. P. & Ries, A. (eds) *Collisional Tectonics*. Geological Society, London, *Special Publications* 19, 321–328.
- DeWaele, B. (2005). The Proterozoic geological history of the Irumide belt, Zambia. Ph.D. thesis, Curtin University of Technology, Perth, 468 pp.
- De Waele, B. & Fitzsimons, I. C. W. (2004). The age and detrital fingerprint of the Muva Supergroup of Zambia: molassic deposition to the southwest of the Ubendian belt. In: *Geoscience Africa 2004, Johannesburg, South Africa*, pp. 162–163.
- De Waele, B., Wingate, M. T. D., Mapani, B. & Fitzsimons, I. C. W. (2003). Untying the Kibaran knot: a reassessment of Mesoproterozoic correlations in southern Africa based on SHRIMP U–Pb data from the Irumide belt. *Geology* **31**, 509–512.
- De Waele, B., Liégeois, J. P., Nemchin, A. A. & Tembo, F. (2006a). Isotopic and geochemical evidence of Proterozoic episodic crustal reworking within the Irumide Belt of south-central Africa, the southern metacratonic boundary of an Archaean Bangweulu Craton. *Precambrian Research* **148**, 225–256.
- De Waele, B., Kampunzu, A. B., Mapani, B. & Tembo, F. (2006b). The Irumide belt of Zambia. *Journal of African Earth Sciences* **46**, 36–70.
- Evans, R. J., Ashwal, L. D. & Hamilton, M. A. (1999). Mafic, ultramafic and anorthosite rocks of the Tete complex, Mozambique: petrology, age and significance. *South African Journal of Geology* **102**, 153–166.
- Goldstein, S. L., O’Nions, R. K. & Hamilton, P. J. (1984). A Sm–Nd study of atmospheric dusts and particulates from major river systems. *Earth and Planetary Science Letters* **70**, 221–236.
- Goscombe, B., Fey, P. & Both, F. (1994). Structural evolution of the Chewore Inliers, Zambezi Mobile Belt, Zimbabwe. *Journal of African Earth Sciences* **19**, 199–224.
- Goscombe, B., Armstrong, R. A. & Barton, J. M. (1998). Tectonothermal evolution of the Chewore Inliers: partial re-equilibration of high-grade basement during the Pan-African Orogeny. *Journal of Petrology* **39**, 1347–1384.
- Goscombe, B., Armstrong, R. A. & Barton, J. M. (2000). Geology of the Chewore Inliers, Zimbabwe: constraining the Mesoproterozoic to Palaeozoic evolution of the Zambezi belt. *Journal of African Earth Sciences* **30**, 589–627.
- Hanson, R. E. (2003). Proterozoic geochronology and tectonic evolution of southern Africa. In: Yoshida, M., Windley, B. F., & Dasgupta, S., (eds) *Proterozoic East Gondwana: Supercontinent Assembly and Breakup*. Geological Society, London, *Special Publications* **206**, 427–463.
- Humphris, S. E. & Thompson, G. (1978). Trace element mobility during hydrothermal alteration of oceanic basalts. *Geochimica et Cosmochimica Acta* **42**, 127–136.
- Iizuka, T. & Hirata, T. (2005). Improvements of precision and accuracy in *in situ* Hf isotope microanalysis of zircon using the laser ablation-MC-ICPMS technique. *Chemical Geology* **220**, 121–137.
- Janousek, V., Farrow, C. M. & Erban, V. (2006). Interpretation of whole-rock geochemical data in igneous geochemistry: introducing Geochemical Data Toolkit (GCDkit). *Journal of Petrology* **47**, 1255–1259.
- John, T., Schenk, V., Mezger, K. & Tembo, F. (2004). Timing and *PT* evolution of whiteschist metamorphism in the Lufilian Arc–Zambezi belt Orogen (Zambia): implications for the assembly of Gondwana. *Journal of Geology* **112**, 71–90.
- Johnson, S. P. & Oliver, G. J. H. (2000). Mesoproterozoic oceanic subduction, island-arc formation and the initiation of back-arc spreading in the Kibaran belt of central, southern Africa: evidence from the ophiolite terrane, Chewore inliers, northern Zimbabwe. *Precambrian Research* **103**, 125–146.
- Johnson, S. P. & Oliver, G. J. H. (2002). High fO_2 metasomatism during whiteschist metamorphism. *Journal of Petrology* **43**, 271–290.
- Johnson, S. P. & Oliver, G. J. H. (2004). Tectonothermal history of the Kaourera Arc, northern Zimbabwe: implications for the tectonic evolution of the Irumide and Zambezi Belts of south central Africa. *Precambrian Research* **130**, 71–97.
- Johnson, S. P., Rivers, T. & De Waele, B. (2005). A review of the Mesoproterozoic to early Palaeozoic magmatic and tectonothermal history of south-central Africa: implications for Rodinia and Gondwana. *Journal of the Geological Society, London* **162**, 433–450.
- Johnson, S. P., De Waele, B. & Liyungu, K. (2006). U–Pb SHRIMP zircon geochronology of granitoid rocks in eastern Zambia: terrane subdivision of the Mesoproterozoic Southern Irumide Belt. *Tectonics* **25**, TC6004, doi:10.1029/2006TC001977.
- Johnson, S. P., DeWaele, B., Evans, D., Banda, W., Tembo, F., Milton, J. A., and Tani, K. (2007). Geochronology of the Zambezi Supracrustal Sequence, Southern Zambia: A Record of Neoproterozoic divergent processes along the Southern Margin of the Congo Craton. *The Journal of Geology* **115**, 355–374.
- Kröner, A., Pidgeon, R. J., Sacchi, R. & Windley, B. F. (1997). Single zircon ages from high-grade gneisses of the Mozambique Belt in

- Malawi, northern Mozambique and Madagascar: evidence for Pan-African metamorphism and implications for Gondwana assembly. *Terra Nova* **9**, Abstracts Supplement 1, 163.
- Ludwig, K. R. (2001a). *Isoplot/Ex rev. 2.49*. Berkeley Geochronology Centre Special Publication.
- Ludwig, K. R. (2001b). *Squid 1.02: a User's Manual. 2*. Berkeley Geochronology Centre Special Publication.
- Mäkitie, H., Lehtonen, M. I., Manninen, T., Koistinen, T., Eerola, T. & Mänttari, I. (2006). New data of granitoids from northern Tete Province, Mozambique. In: *21st Colloquium of African Geology, Maputo, Mozambique, July 2006*, pp. 109–110.
- Mänttari, I., Koistinen, T., Lehtonen, M. I., Manninen, T., Mäkitie, H., Huhma, H. & Kuosmanen, E. (2006). U–Pb and Sm–Nd ages for 27 magmatic rocks, NW Mozambique. In: *21st Colloquium of African Geology, Maputo, Mozambique, July 2006*, pp. 203–205.
- Mapani, B. S. E., and Moore, T. A. (1995). The geology of the Serenji area, explanation of degree sheet 1330 NW quarter. Lusaka: Geological Survey Department of Zambia.
- Mapani, B. S. E., Rivers, T., Tembo, F. & Katongo, C. (2001). Terrane mapping in the eastern Irumide and Mozambique belts: implications for the assembly and dispersal of Rodinia. In: McCourt, S. (ed.) *IGCP 418 4th Field Meeting, University of Durban–Westville, Durban, South Africa*.
- Mapani, B., Rivers, T., Tembo, F., De Waele, B. & Katongo, C. (2004). Growth of the Irumide terranes and slices of Archaean age in eastern Zambia. In: *Geoscience Africa 2004, Johannesburg, South Africa*, pp. 414–415.
- Meschede, M. (1986). A method of discriminating between different types of mid-ocean ridge basalts and continental tholeiites with the Nb–Zr–Y diagram. *Chemical Geology* **56**, 207–218.
- Nakamura, N. (1974). Determination of REE, Ba, Fe, Mg, Na and K in carbonaceous and ordinary chondrites. *Geochimica et Cosmochimica Acta* **38**, 757–775.
- Nelson, D. R. (1996). Compilation of SHRIMP U–Pb zircon geochronology data, 1995. *West Australian Geological Survey, Record* **1996/5**, 168 pp.
- Oliver, G. J. H., Johnson, S. P., Williams, I. S. & Herd, D. A. (1998). Relict 14 Ga oceanic crust in the Zambezi Valley, northern Zimbabwe: evidence for Mesoproterozoic supercontinental fragmentation. *Geology* **26**, 571–573.
- Patchette, P. J., Kuovo, O., Hedge, C. E. & Tatsumoto, M. (1981). Evolution of the continental crust and mantle heterogeneity: evidence from Hf isotopes. *Contributions to Mineralogy and Petrology* **78**, 279–297.
- Pearce, J. A. (1983). Role of the sub-continental lithosphere in magma genesis at active continental margins. In: Hawkesworth, C. J. & Norry, M. J. (eds) *Continental Basalts and Mantle Xenoliths*. Nantwich: Shiva, pp. 230–249.
- Pearce, J. A. & Cann, J. R. (1973). Tectonic setting of basic volcanic rocks determined using trace element analyses. *Earth and Planetary Science Letters* **19**, 209–300.
- Pearce, J. A. & Norry, M. J. (1979). Petrogenetic implications of Ti, Zr, Y and Nb variations in volcanic rocks. *Contributions to Mineralogy and Petrology* **69**, 33–47.
- Rubatto, D. & Gebauer, D. (2000). Use of cathodoluminescence for U–Pb zircon dating by ion microprobe: some examples from the Western Alps. In: Pagel, M., Barbin, V., Blanc, P. & Ohnenstetter, D. (eds) *Cathodoluminescence in Geosciences*. Berlin: Springer, pp. 373–400.
- Schenk, V. & Appel, P. (2001). Anti-clockwise *P–T* path during ultrahigh-temperature (UHT) metamorphism at *c.* 1050 Ma in the Irumide Belt of Eastern Zambia. *Berichte der Deutschen Mineralogischen Gesellschaft, Beihefte zum European Journal of Mineralogy* **13**, 161.
- Schenk, V. & Appel, P. (2002). UHT-metamorphism in the Irumide belt of Zambia: an anti-clockwise *P–T* path and concordant monazite age at 1.05 Ga. In: Ennih, N. & Abdelsalam Mohamed, G. (eds) *19th Colloquium of African Geology, El Jadida, Morocco*, 165 pp.
- Scherer, E., Münker, C. & Mezger, K. (2001). Calibration of the lutetium–hafnium clock. *Science* **293**, 683–687.
- Stacey, J. S. & Kramers, J. D. (1975). Approximation of terrestrial lead isotopic evolution by a two-stage model. *Earth and Planetary Science Letters* **26**, 207–221.
- Tani, K., Kawabata, H., Chang, Q., Sato, K. & Tatsumi, T. (2005). Quantitative analyses of silicate rock major and trace elements by X-ray fluorescence spectrometer: evaluation of analytical precision and preparation. *Institute for Earth Evolution Annual Report*.
- Thirlwall, M. & Anczkiewicz, R. (2004). Multidynamic isotope ratio analyses using MC-ICP-MS and the causes of secular drift in Hf, Nd and Pb isotope ratios. *International journal of Mass Spectrometry* **235**, 59–81.
- Thomas, J. B., Bodnar, R. J., Shimizu, N. & Chesnar, C. A. (2003). Melt inclusions in zircon. In: Hanchar, J. M. & Hoskin, P. W. O. (eds) *Zircon. Mineralogical Society of America, Reviews in Mineralogy and Geochemistry* **53**, 63–87.
- Winchester, J. A. & Floyd, P. A. (1977). Geochemical discrimination of different magma series and their differentiation products using immobile elements. *Chemical Geology* **20**, 325–343.
- Wood, D. A. (1980). The application of a Th–Hf–Ta diagram to problems of tectonomagmatic classification and to establishing the nature of crustal contamination in basaltic lavas of the British Tertiary volcanic province. *Earth and Planetary Science Letters* **50**, 11–30.